Wide Discrepancies in the Magnitude and Direction of Modelled SIF in Response to Light Conditions

Nicholas C Parazoo[1], Troy Magney[1,2], Alex Norton[3], Brett Raczka[4], Cédric Bacour[5], Fabienne Maignan[6], Ian Baker[7], Yongguang Zhang[8], Bo Qiu[8], Mingjie Shi[9], Natasha MacBean[10], Dave R. Bowling[4], Sean P. Burns[11,12], Peter D. Blanken[11], Jochen Stutz[9], Katja Grossman[13], Christian Frankenberg[1,2]

Jet Propulsion Laboratory, California Institute of Technology[1]

California Institute of Technology[2]

School of Earth Sciences, University of Melbourne[3]

School of Biological Sciences, University of Utah[4]

NOVELTIS, 153 rue du Lac, 31670 Labège, France[5]

Laboratoire des Sciences du Climat et de l'Environnement, LSCE/IPSL[6]

Colorado State University[7]

International Institute for Earth System Sciences, Nanjing University, China[8]

University of California Los Angeles[9]

Department of Geography, Indiana University[10]

Department of Geography, University of Colorado[11]

National Center for Atmospheric Research[12]

Institute of Environmental Physics, University of Heidelberg[13]

Prepared for Biogeosciences

Abstract:

Recent successes in passive remote sensing of far-red solar induced chlorophyll fluorescence (SIF) have spurred development and integration of canopy-level fluorescence models in global terrestrial biosphere models (TBMs) for climate and carbon cycle research. The interaction of fluorescence with photochemistry at the leaf- and canopy- scale provides opportunities to diagnose and constrain model simulations of photosynthesis and related processes, through direct comparison to and assimilation of tower, airborne, and satellite data. TBMs describe key processes related to absorption of sunlight, leaf-level fluorescence emission, scattering and reabsorption throughout the canopy. Here, we analyze simulations from an ensemble of process-based TBM-SIF models (SiB3, SiB4, CLM4.5, CLM5.0, BETHY, ORCHIDEE, BEPS) and the SCOPE canopy radiation and vegetation model at a subalpine evergreen needleleaf forest near Niwot Ridge, Colorado. These models are forced with local meteorology and analyzed against tower-based continuous far-red SIF and gross primary productivity (GPP) partitioned eddy covariance data at diurnal and synoptic scales during the growing season (July-August 2017). Our primary objective is to summarize the site-level state of the art in TBM-SIF modeling over a relatively short time period (summer) when light, canopy structure, and pigments are similar, setting the stage for regional- to global-scale analyses. We find that these models are generally well constrained in simulating photosynthetic yield, but show strongly divergent patterns in the simulation of absorbed photosynthetic active radiation (PAR), absolute GPP and fluorescence, quantum yields, and light response at leaf and canopy scale. This study highlights the need for mechanistic modeling of non-photochemical quenching in stressed and unstressed environments, and improved representation of light absorption (APAR), distribution of light across sunlit and shaded leaves, and radiative transfer from leaf to canopy scale.

Section 1: Introduction

Our ability to estimate and measure photosynthesis beyond the leaf scale is extremely limited. This inhibits the ability to evaluate the performance of terrestrial biosphere models (TBMs) that are designed to quantify the direct impact and feedbacks of the carbon cycle with climate change. Consequently, there are substantial uncertainties in estimating the gross primary production (GPP) response to environmental changes and carbon-climate feedback (Friedlingstein et al., 2014). Global, multi-scale remote sensing of solar induced fluorescence (SIF) may represent a major breakthrough in alleviating this deficiency (Mohammed et al, 2019). Spaceborne data indicate a linear relationship between SIF and GPP at large spatial (kilometer) and temporal (bi-weekly) scales (e.g., Sun et al., 2017) for several ecosystems, while theoretical models and ground-based measurements indicate a more non-linear relationship at leaf and canopy scales (Zhang et al., 2016; Gu et al., 2019; van der Tol et al., 2014; Magney et al., 2017, 2019a).

Chlorophyll fluorescence is re-emitted energy produced during the photosynthetic light reactions, in which a small fraction (roughly 2%) of photosynthetic active radiation (PAR) absorbed by chlorophyll is re-emitted at longer wavelengths (650-850 nm) as fluorescence. In ambient conditions, the emission of SIF represents a by-product of two primary de-excitation pathways, photochemical and nonphotochemical quenching (PQ, NPQ). Plants have evolved these regulatory mechanisms to prevent damage to photosynthetic machinery when the amount of absorbed radiation is greater than that which can be used to drive photochemistry. Chlorophyll fluorescence responds dynamically to changes in photochemistry and NPQ from instantaneous to hourly, daily, and seasonal timescales, as a function of changing environmental conditions and plant structural properties (Porcar-Castell et al., 2014; Demmig-Adams et al., 2012). SIF is fundamentally different than steady-state fluorescence yield typically measured at the leaf scale as it is sensitive to both changes in photochemistry as well as absorbed PAR (APAR, related to incident light, canopy structure, and biochemical content). The response of canopy SIF to APAR is well documented in deciduous and evergreen forests and cropping ecosystems (Yang et al., 2018; Badgley et al, 2017; Miao et al., 2018; Magney et al., 2019b; Li et al., 2020). More recently, Magney et al. (2019b) showed that seasonal changes in canopy SIF for cold climate evergreen

78 systems is influenced by changes in needle physiology and photoprotective pigments (Magney et
79 al., 2019b).

80 To properly account for these factors, process-based SIF models must represent these underlying
81 non-linear biophysical and chemical processes. Several modeling groups have adapted TBMs to
82 incorporate various SIF formalisms for the purpose of model evaluation, data assimilation, and
83 improved model prediction (Lee et al., 2015; Koffi et al., 2015; Thum et al., 2017; Norton et al.,
84 2019; Bacour et al., 2019; Raczka et al., 2019). With these goals in mind, TBM SIF modeling
85 requires two important steps: (1) a representation of SIF at the leaf scale that accounts for NPQ
86 and photochemistry, and (2) canopy radiative transfer of SIF, which enables a comparison to large
87 field-of-view observations (e.g. tower, satellites). The second step involves accounting for
88 radiative transfer within the canopy and has typically relied on incorporating the Soil Canopy
89 Observation Photosynthesis Energy model (SCOPE, van der Tol et al., 2009, 2014), which
90 simulates chlorophyll fluorescence as a function of biophysics, canopy structure, environmental
91 conditions, and sun/sensor geometries. This approach has been adopted by TBMs in various ways
92 using different assumptions for fluorescence modeling and radiative transfer, as will be discussed
93 in Section 2.

94 Typically, measuring chlorophyll fluorescence and competing pathways (PQ, NPQ) has been done
95 at the leaf scale via pulse-amplitude modulation fluorescence (PAM, Schreiber et al., 1986).
96 Recently, commercially available spectrometers have made it possible to measure SIF directly in
97 the field at the leaf and canopy scale, and also enable the study of structural, environmental, and
98 directional controls (Cogliati et al. 2015; Daumard et al. 2010; Migliavacca et al. 2017; Yang et al.
99 2015; Grossman et al., 2018; Aasen et al., 2019; Gu et al., 2019b; Zhang et al., 2019). The use of
100 field deployable instruments on eddy covariance towers has increased rapidly since 2014,
101 providing coverage of multiple vegetation types across various climates around the world (Yang
102 et al., 2018; Magney et al., 2019a,b; Parazoo et al., 2019). These data enable improved
103 understanding of the relationship between SIF, GPP, APAR, and environmental effects at canopy
104 scales. Novel tower-mounted spectrometer systems such as Fluospec2 (Yang et al., 2018),
105 Photospec (Grossman et al., 2018), and FLOX (e.g., Julitta et al., 2017; Shan et al., 2019) have
106 made it possible to monitor canopy SIF continuously in the field with high precision over multiple

years providing opportunities for more direct comparison and evaluation of satellite data (Grossman et al., 2018; Yang et al., 2015, 2018; Wohlfahrt et al., 2018; Magney et al., 2019b). PhotoSpec offers the additional benefits (and challenge) of (a) precise field of view capable of resolving leaf-level SIF, and (b) canopy scanning at azimuth and elevation angles. These features enable SIF integration from leaf- to canopy- scales, and interpretation of directional variations of the emitted radiance.

Canopy scanning spectrometers such as PhotoSpec thus provide an opportunity to understand the physical processes that lead to a breakdown of SIF-GPP linearity at leaf to canopy scale (or conversely, emergence of linearity at increasing scale), and for detailed evaluation and diagnosis of TBM performance. This study provides a preliminary benchmarking site-level assessment for simulations of SIF within a TBM framework and across an ensemble of TBMs, with the primary purpose being an initial investigation into the response of modelled SIF and GPP to light during peak summer. We leverage continuous measurements of SIF and GPP at the Niwot Ridge US-NR1 Ameriflux flux tower in Colorado from June-July 2017 (Magney et al., 2019b), and simulations of canopy radiative transfer, photosynthesis, and fluorescence from a stand-alone version of SCOPE, to (1) Benchmark TBM-SIF modeling, (2) Evaluate sensitivity to underlying processes and scaling techniques, (3) Identify strengths and weaknesses in current modeling strategies, and (4) Recommend strategies for models and observations.

The paper is organized as follows: Section 2 describes SCOPE and the seven TBM-SIF models (SiB3, SiB4, ORCHIDEE, BEPS, BETHY, CLM4.5, CLM5) which have recently been published or are in review, and provides more details on site level benchmarking observations. Section 3 summarizes results comparing modelled and predicted SIF and GPP at hourly and daily scales, as they relate to absorbed light, GPP and SIF yields, and quantum yields. Section 4 discusses results in more detail, including attribution of SIF magnitude and temporal phasing biases and sensitivities to absorbed light, and areas for improvement.

Section 2: Methods

2.1 Site: Niwot Ridge, Colorado

Our study focuses on an AmeriFlux (https://ameriflux.lbl.gov/) site in Niwot Ridge, Colorado, USA (US-NR1), where a tower-based eddy covariance system has been continuously measuring the net ecosystem exchange of carbon dioxide (NEE) over a high-elevation subalpine forest since 1999, and a spectrometer system that has been continuously monitoring SIF since June 2017 (Grossman et al., 2018; Magney et al., 2019b). The 26 m tall tower is located in a high elevation forest (3050 m asl) located in the Rocky Mountains of Colorado (Burns et al., 2015; Hu et al., 2010; Monson et al., 2002) and consists primarily of the evergreen species of lodgepole pine (*Pinus contorta*), Engelmann spruce (*Piceae engelmanii*), and subalpine fir (*Abies lasiocarpa*). The mean annual temperature is 1.5°C and mean annual precipitation is 800 mm (65% as snow). The forest is roughly 120 years old with a mean canopy height of 11.5 m, and a leaf area index of 4.2 m^2 m^{-2}. More site-specific details can be found in Burns et al. (2015).

At Niwot Ridge, interannual variations in GPP are closely linked to winter snowfall amount, which typically melts by early June, and summer precipitation, characterized by afternoon convective thunderstorms triggered by upslope flow (Burns et al., 2015; Albert et al., 2017) and climatological peak precipitation around 2 pm local time (Fig 1A). We note that our study period of July-August 2017 is unusual for NR1 (relative to the 2015-2018 mean) in its bimodal distribution of diurnal precipitation (morning and afternoon peaks), lower than normal afternoon precipitation, cooler temperatures, and reduced vapor pressure deficit (Fig 1 A-C). The early morning peak is due to a strong storm system that moved through from July 22-24 (Fig 1E), and does not show up when these days are removed. This period also shows a decrease in incoming shortwave relative to climatology despite lower precipitation (Fig 1D). We note that a second storm passed through in early August. The combination of these two storms produced net decreases in air temperature (Fig 1F), vapor pressure deficit (Fig 1G) and sunlight (Fig 1H) over a two-week period from late July to early August.

2.2 Tower-Based Measurements: PAR, SIF, CO_2 Flux

2.2.1 Absorbed PAR

The site is equipped with two main upward-facing PAR sensors. The first (LICOR LI-190R), mounted on the PhotoSpec telescope unit, provides an independent measurement of

direct/diffuse light and can be used to calibrate PhotoSpec (Grossman et al., 2018). The second (SQ-500-SS; Apogee Instruments), mounted on the main flux tower, is part of a larger array of upward- and downward-oriented PAR sensors above and below the canopy used for the calculation of the fraction of PAR absorbed by the vegetation canopy (fAPAR). The two PAR sensors show a similar diurnal pattern during July-August 2017 (Fig S1), including an afternoon dip and relatively smaller values overall compared to 2018 (the only other year with available PAR for comparison).

Full-spectrum quantum sensors (SQ-500-SS; Apogee Instruments) were new and factory-calibrated together just before installation. Above-canopy sensors (one up and one down-facing) were mounted on the main flux tower, and below-canopy sensors (six up and six down) were mounted at the 2 m height above ground on a shorter canopy-access towers. APAR was calculated for each pair of below-canopy relative to above-canopy sensors for every half-hour, then averaged among sensors over daylight hours to create a daytime average. We then estimate hourly APAR by multiplying hourly incoming PAR (measured and integrated from 400-700 nm) at the top of canopy (PAR) by the daytime average of fAPAR. Fig S2 shows the mean diurnal cycle for July-August 2017 for each sensor, and the across-sensor average, with APAR data collection beginning on July 13, 2017. We note that APAR measurements are only as representative as the distribution of PAR sensors beneath the canopy; while they are placed within the footprint of SIF (Sec 2.2.3) and fetch of eddy covariance (Sec 2.2.4) measurements, they cannot be a perfect representation of canopy APAR for each eddy covariance and SIF measurement.

2.2.2 Fluorescence parameters

We define and clarify three important quantities that define the relationship between absorbed light and emitted SIF at leaf and canopy scales. ϕ_F is the quantum yield of fluorescence, representing the probability an absorbed photon will be fluoresced. This quantity can be observed at leaf level using PAM fluorimetry or calculated by models as a function of rate coefficients for energy transfer (Sec 2.3.3). SIF_{yield} is the canopy emitted SIF per photon absorbed. The quantity is estimated from models and observations as the ratio of absolute canopy SIF and APAR (SIF_{canopy}/APAR). SIF_{yield} is our best attempt to account for the effects of (a) canopy absorbed light and (b) SIF re-absorption within the canopy on the canopy integrated emission of SIF.

However, factors such as observation angle, fraction of sunlit/shaded canopy components, and difference in footprint from APAR, necessitates an additional diagnostic variable defined as relative SIF (SIF_{rel}). SIF_{rel} is emitted SIF per reflected radiance in the far red spectrum where SIF retrievals occur (SIF/Ref_{fr}). This is useful because is normalizes for the exact amount of 'illuminated' canopy components within the sensor field of view, whereas APAR measurements are integrated for the entire canopy.

These quantities represent different but equally important versions of reality. It is difficult for models to exactly reproduce the distribution and timing of sunlight in the canopy as observed by PhotoSpec. While SIF_{rel} removes model-observation differences in illumination, it confounds our interpretation of the relationship with GPP_{yield}, which is derived from APAR. As such, we provide both results to be comprehensive, but note the temporal stability associated with SIF_{rel} as the more physical interpretation of canopy yield for this short period of study.

2.2.3 Tower Based Measurements of Solar Induced Chlorophyll Fluorescence (SIF)

SIF data has been collected from a scanning spectrometer (PhotoSpec) installed at the AmeriFlux US-NR1 tall tower since June 17, 2017. PhotoSpec sits atop the tower at 26 m above the ground and roughly 15 m above the forest canopy top, transferring reflected sunlight and SIF data collected from the needleleaf canopy through a tri-furcated optical cable to three spectrometers in a shed at the base of the tower. These spectrometers measure far-red fluorescence in the 745-758 nm retrieval window at high spectral resolution (FWHM = 0.3 nm) and with a 0.7 deg field of view (FOV), resulting in a 20 cm diameter footprint at nadir on top of the canopy. The far-red SIF data are then scaled to 740 nm for model intercomparison using the first principal component of the spectral shape in Magney et al., 2019a. Photospec scans from nadir to the horizon in 0.7 degrees steps at two azimuth directions, with a time resolution of ~20 s per measurement and complete scan time of 20 minutes. For this study, we aggregate scans across all azimuth and elevation angles into hourly, canopy level averages to benchmark model estimates of top of canopy (TOC) or canopy averaged SIF (BETHY only, see Sec *2.3.4.*1) at diurnal and synoptic time scales. We refer the reader to Grossman et al. (2018) and Magney et al (2019b) for further details regarding PhotoSpec, implementation at US-NR1, and data filtering, and to Magney et al (2019c)

for data access. We focus our model-data analysis on the 2017 growing season (July-August, 2017) to maximize overlap between observations of SIF, GPP, and APAR.

Diurnal composites of PhotoSpec SIF in 2017 show a late morning peak and afternoon dip (Fig S3A). The afternoon dip is consistent with decreased incoming shortwave, PAR and APAR (Figs S1 and S2, respectively). However, we note the retrieved signal from PhotoSpec is also affected by (1) viewing geometry, (2) fraction of sunlit vs shaded leaves (sun/shade fraction, i.e. the quantity of needles illuminated by incident sunlight) due to self-shading within the canopy, and (3) direct/diffuse fraction due to cloud cover. Structural and bidirectional effects lead to different SIF emission patterns depending on view angle and scanning patterns (Yang and van der Tol, 2018). The viewing geometry of PhotoSpec (as implemented at NR1 in 2017) causes a higher fraction of illuminated vegetation in the morning, which leads to a 2 to 3 hour offset in the timing of peak SIF (Fig S3A) and incoming far-red reflected radiance within the retrieval window (Fig S3B), from the peak zenith angle of the sun at noon (coinciding with the expected peak in PAR) to late morning. Normalizing SIF by far-red reflected radiance as relative SIF (SIF_{rel}, Fig S3C) and rescaling to SIF (Fig S3D) shifts the peak back to noon and preserved the afternoon dip (albeit with reduced magnitude). SIF_{rel} helps to account for factors 1-3 listed above because it accounts for the amount of reflected radiation in the field of view of PhotoSpec, which is impacted by canopy structure, sun angle, and direct/diffuse light. As discussed above, SIF_{rel} is likely a better approximation of SIF_{yield} because it normalizes for the exact amount of 'illuminated' canopy components in each retrieval, whereas APAR integrates the entire canopy. As such, we expect SIF_{rel} to have a strong seasonal change associated with downregulation of photosynthesis, and a more subtle diurnal change, as during mid-summer the SIF signal is primarily driven by light intensity.

It is important to note that the PhotoSpec system is highly sensitive to sun/shade fraction in the canopy (factor 2) due to the narrow FOV of the PhotoSpec telescoping lens. Increased afternoon cloud cover during summer causes diurnal asymmetry in incident PAR (Fig S1A). We examine this effect in more detail (Section 3) by analyzing SIF and GPP under clear and diffuse sky conditions using a threshold (0.5, top-of-canopy/top-of-atmosphere incoming shortwave radiation) similar to that used in Yang et al. (2017) and Yang et al. (2018).

2.2.4 CO_2 Flux and GPP Partitioning

NEE measurements are screened using u_{star} filtering, and partitioned into gross primary production (GPP) and terrestrial ecosystem respiration components using the so-called nighttime method which is based on the relationship between NEE during the nighttime (PAR < 50 umol m^{-2} s^{-1}) and air temperature (Reichstein et al., 2005). Diurnal averages of GPP based on nighttime partitioning show similar diurnal structure to PAR and SIF including the afternoon dip and reduced overall magnitude compared to the 2015-2018 mean (Fig S4). Similar results are found using daytime light partitioning of NEE (Lasslop et al., 2010; Fig S4) and thus only nighttime partitioned GPP data are reported for the remainder of this study. All GPP estimates are processed as half hourly means, then gap filled and averaged hourly. We note the tower location near the Continental Divide in the Rocky Mountains of Colorado presents slope flow challenges for eddy covariance during nighttime, but the relatively flat area of the tower reduces impact on daytime flux measurements (Burns et al., 2018). Details on the flux measurements, data processing and quality control are provided in Burns et al. (2015).

2.3 Modeling Approach

2.3.1 TBM-SIF Overview

The parent TBMs are designed to simulate the exchanges of carbon, water, and energy between biosphere and atmosphere, from global to local scales depending on inputs from meteorological forcing, soil texture, and plant functional type. The addition of a fluorescence model that simulates SIF enables a direct comparison to remotely sensed observations for benchmarking, process diagnostics, and parameter/state optimization (data fusion) for improved GPP estimation. The TBM-SIF models analyzed here differ in ways too numerous to discuss. We refer the reader to the appropriate references in Section 2.3.4 for more detailed model descriptions. Instead, we focus on key differences affecting joint simulation of GPP and leaf/canopy level SIF at diurnal and synoptic scale, during the peak of summer. These differences, which are summarized in Table 1, include the representation of stomatal-conductance (all use Ball-Berry except CLM5.0, BEPS, and ORCHIDEE), canopy absorption of incoming radiation (all account for sunlit/shaded radiation except ORCHIDEE, SiB3, and SiB4), limiting factors for photosynthesis

(V_{cmax}, LAI, radiation, stress) and SIF (k_N, fluorescence photon re-absorption), scaling and radiative transfer methods for transferring leaf-level SIF simulations to top of canopy, and parameter optimization. Further details on (a) photosynthetic structural formulation and parameter choice, (b) representation of leaf level processes important to SIF (k_N and ϕ_P), and (c) leaf-to-canopy scaling approach (SIF_{canopy}) are provided in Sections 2.3.2 and 2.3.3.

2.3.2 Photosynthesis Models

All TBM-SIF models in this manuscript used enzyme-kinetic models to simulate leaf assimilation rate (gross photosynthesis) as limited by the efficiency of photosynthetic enzyme system, the amount of PAR captured by leaf chlorophyll, and the capacity of leaves to utilize end products of photosynthesis (Farquhar et al., 1980; Collatz et al., 1991, 1992; Sellers et al., 1996). However, there are important differences in the representation of (a) stomatal conductance that couples carbon/water cycles, and (b) limiting factors on carbon assimilation due to leaf physiology (maximum carboxylation capacity, V_{cmax}), radiation (APAR or fAPAR), canopy structure (LAI, leaf angle distribution), and stress (water supply and demand, temperature), that affect plant physiological processes and canopy radiative transfer. The underlying stomatal conductance models in the TBMs analyzed here are represented by the Ball-Berry family of empirical models rooted in the leaf gas exchange equation but with different representations of atmospheric demand (relative humidity or vapor pressure deficit), including the Ball-Berry-Woodrow model (Ball et al., 1987), the Leuning model (Leuning, 1995), the Yin-Stuik model (Yin and Struik, 2009), and the Medlyn model (Medlyn et al., 2011). These structural and parametric differences also influence calculated values such as the degree of light saturation (Section 2.3.3), which influence both the fluorescence and quantum yield as used by the fluorescence models. Differences in stomatal conductance, canopy type / radiation scheme, stress, V_{cmax}, and LAI are summarized in Table 1.

2.3.3 Fluorescence Modeling Approach

Following the general approach described in Lee et al. (2015) and van der Tol et al. (2014), the flux of total leaf-level emitted fluorescence, SIF_{leaf}, can be diagnosed using a light use efficiency framework analogous to the expression for photosynthesis (Monteith et al., 1972),

$$SIF_{leaf} = fAPAR * PAR * \phi_F$$

$$= APAR * \phi_F \quad \textit{Equation 1}$$

where *PAR* and *fAPAR* are defined in Section 2.2.1 but measured at leaf level, and ϕ_F is the quantum yield of fluorescence, representing the number of photons emitted by fluorescence per absorbed photon. We note that photosystems I and II (PS1 and PSII, respectively) contribute to leaf level fluorescence but only PSII is considered in models analyzed here (with the exception of ORCHIDEE and BETHY, Section 2.3.4.2). ϕ_F is estimated as follows:

$$\phi_F = \frac{k_F}{k_F + k_D + k_N}(1 - \phi_P) \quad \textit{Equation 2}$$

where *k* represents the rate coefficients for the different pathways for the transfer of energy from excited chlorophyll (k_F = fluorescence, k_D = heat dissipation, and k_N = non-photochemical quenching, or NPQ), and ϕ_P is the quantum yield of electron transport (see Section 2.3.2). k_F is typically set to a constant value (0.05) in models following van der Tol et al (2014). k_D is also typically set to a constant value of 0.95, or temperature corrected in some cases (e.g., ORCHIDEE, CLM4.5, CLM5.0, BETHY). k_N has a substantial and variable impact on energy partitioning at diurnal and seasonal scales which varies as a function of light saturation (e.g., Raczka et al., 2019; Porcar-Castell et al., 2011). Once leaf level emissions are known, an approach is needed estimate the total TOC fluorescence flux (SIF_{canopy}) for comparison to Photospec data. Leaf and canopy level fluorescence modeling is described in more detail in Section 2.3.3.1 and 2.3.3.2 below.

2.3.3.1 Leaf level SIF emission

The 'quantum yield' approach has been used in SIF models to characterize the fraction of photons that are used for PQ, NPQ, or re-emitted as fluorescence (van der Tol 2014). It is important to note, that this does not translate into the actual amount of SIF emission leaving the leaf, but is used as an approximation. TBM-SIF models typically represent ϕ_P using lake model formalism, which assumes large connectivity between photosynthetic units (Genty et al., 1989; van der Tol et al., 2014). ϕ_P is expressed in terms of the degree of light saturation (*x*), derived from the native photosynthesis module of the parent TBM and represents the balance between actual and potential electron transport rates, and the maximum photochemical yield under dark-acclimated

conditions (ϕ_{Pmax}), which is derived from the fluorescence model and defined in terms of rate coefficients in Eq 2.

ϕ_N accounts for the ability of plants to dissipate excess energy as heat via NPQ through the regulation of xanthophyll cycle pigments (Demmig-Adams and Adams, 2006). NPQ can be represented as a sum of reversible (k_R) and sustain (k_S) components ($k_N = k_R + k_S$). k_R accounts for the relatively fast (diurnal), reversible NPQ response to light. k_S accounts for the relatively slow (seasonal), sustained NPQ response to light and other environmental factors. With the exception of CLM4.5, models do not typically account for k_S.

A significant challenge in fluorescence models is to find an appropriate relationship between k_N and the degree of light saturation (x). The TBM-SIF models represent k_N through an approach similar to the one used in SCOPE, which uses a parametric model of k_N derived from PAM fluorometry measurements (van der Tol et al., 2014).

NPQ models can be classified as stressed (drought) and unstressed relative to water availability depending on the dataset from which empirical fits are derived. The unstressed model is ideal for irrigated systems such as crops, and the stressed model is more appropriate for water limited ecosystems such as Niwot Ridge. We examine each of these models using drought and unstressed models from van der Tol (2014), and a drought-based model from Flexas et al. (2002). These models use different empirical fits but are otherwise identical. In general, k_N increases more rapidly with APAR (light saturation), and ramps up to a higher level, in the drought-based model compared to the unstressed model. Additionally, some models provide unique improvements such as dependence on environmental conditions (e.g., water stress vs no water stress in ORCHIDEE), and equations for reversible and sustained NPQ to represent the different time scales (minutes to seasonal) at which NPQ regulation occurs (e.g., CLM4.5) influenced by pigmentation changes in the leaf.

2.3.3.2 Leaf-to-Canopy scaling

The TBM-SIFs produce leaf-level fluorescence which needs to be converted to canopy-level fluorescence (SIF_{canopy}) to be directly compared to PhotoSpec and satellite observations. Leaf- to canopy- level conversion of SIF requires a representation of canopy radiative transfer, which in

general is too computationally expensive to include within the TBMs in this study, that are designed for global scale application. Therefore, most TBMs analyzed here account for canopy radiative transfer of SIF using some representation of SCOPE (van der tol 2009a,b). The most commonly used approach is to run independent simulations of SIF from SCOPE to create an empirical conversion factor (κ_{740}) between leaf and canopy level SIF that is a function of V_{cmax} (Lee et al., 2015). This conversion factor accounts for integration over the fluorescence emission spectrum, observation angle, and unit conversion. Model variations of this empirical approach, as well additional approaches utilizing the full SCOPE model and a SCOPE emulator, are summarized below and in Table 1.

2.3.4 TBM-SIF Models

Here we provide a brief description of individual TBM-SIF models and within model experiments. We point out key differences in modeling of photosynthesis, fluorescence, and leaf-to-canopy scaling. We note that within model experiments, labeled as Experiment 1 (exp1), Experiment 2 (exp2), etc, represent increasing order of realism, rather than a specific set of conditions common across models. As such, Experiment 1 in BETHY (*BETHY-exp1*) is not equivalent to Experiment 1 in CLM4.5 (*CLM4.5-exp1*).

2.3.4.1 BETHY

The Biosphere Energy Transfer HydrologY (BETHY) model is the land surface component of the Carbon Cycle Data Assimilation System (CCDAS) developed to ingest a range of observational data for estimating terrestrial carbon fluxes at global scale (Rayner et al., 2005; Kaminski et al., 2013; Koffi et al., 2012; Anav et al., 2015). Koffi et al. (2015) was the first to combine a process-based model of SIF with a global TBM. The native canopy radiative transfer and photosynthesis schemes of BETHY were effectively replaced with corresponding schemes and fluorescence model from SCOPE (Koffi et al., 2015), thus enabling spatially explicit simulation of GPP and SIF as a function of plant function type. This model was extended to include a module for prognostic leaf growth (Norton et al., 2018) and more recently adapted with a formal optimization algorithm for assimilating spaceborne SIF data (Norton et al., 2019). It has been updated for this study to accept hourly meteorological forcing. BETHY-SCOPE, denoted here as BETHY, remains the first and only

global TBM-SIF model to simulate vertically integrated (1-D) fluorescence radiative transfer and energy balance.

We include three experiments to examine the impact of calibrating the k_N model against PAM fluorometry data to different species: (1) *BETHY-exp1* is adapted to unstressed cotton species (van der Tol et al., 2014), (2) *BETHY-exp2* is adapted to drought stressed Mediterranean species (i.e., vineyard in controlled environment subjected to drought) including higher temperature correction (Flexas et al., 2002; van der Tol et al., 2014), (3) *BETHY-exp3* is adapted to drought stressed Mediterranean species (Flexas et al., 2002).

We further leverage SCOPE enabled SIF modeling in BETHY (*BETHY-exp3* specifically) to examine (a) leaf and canopy level SIF and quenching under sunlit and shaded leaves, and (b) SIF emissions at the top of canopy (SIF_{canopy}) versus the average emission within the canopy (SIF_{ave}), which accounts for the average emission from sunlit and shaded leaves. The latter analysis facilitates comparison to PhotoSpec, which observes the entire canopy.

An important caveat in the analysis of BETHY simulations is that, at the time of this writing, the prescribed meteorological forcing at NR1 is only available for 2015. While this degrades comparison to diurnal and synoptic variation observed by PhotoSpec in 2017, we find that analysis of magnitude, light sensitivities, and within model experiments still provides useful insight for interpretation of other TBM-SIFs, and future modeling requirements in general.

2.3.4.2 ORCHIDEE

The Organizing Carbon and Hydrology In Dynamic Ecosystems (ORCHIDEE) model (Krinner et al., 2005) is the land surface component of the Earth System Model of Institut Pierre-Simon Laplace IPSL-CM, (Dufresne et al., 2013) involved in recent exercises of the Coupled Model Intercomparison Project (CMIP) established by the World Climate Research Programme (https://www.wcrp-climate.org/wgcm-cmip). Recently a mechanistic SIF observation operator was developed for ORCHIDEE to simulate the regulation of photosystem II ϕ_F at the leaf level using a novel parameterization of NPQ as a function of temperature, PAR, and normalized ϕ_P. It emulates the radiative transfer of SIF to the top of the canopy using a parametric simplification of SCOPE. The details of the SIF modelling approach are provided in Bacour et al. (2019).

We include three experiments to examine the impact of water stress and parameter optimization (using OCO-2 SIF, see Section 2.4): (1) *ORCHIDEE-exp1* is the standard configuration with default parameters, (2) *ORCHIDEE-exp2* is the same as *ORCHIDEE-exp1* with two key differences (a) water stress is applied to stomatal conductance, mesophyll conductance and to the photosynthetic capacity, and (b) the tree height (12 m instead of 15 m) was set specifically for the NR1 site, (3) *ORCHIDEE-exp3* is the same as *ORCHIDEE-exp1* but includes OCO-2 optimized parameters.

2.3.4.3 BEPS

The Boreal Ecosystem Product Simulator (BEPS) is an enzyme kinetic two-leaf model for simulating carbon and water cycles for different plant functional types (Chen et al., 1999; Liu et al., 2003). BEPS uses a modified Ball-Berry stomatal conductance model (Leuning et al., 1995) and semi-analytical canopy radiative transfer. The canopy architecture is well considered in BEPS model, which has not only remote-sensed LAI but also the global map of the foliage clumping index. The fluorescence emission at the leaf level follows the approach of Lee et al (2015). SIF emission for sunlit and shaded leaves are separately simulated based on illumination and canopy geometry in BEPS. In addition, multiple scattering SIF is also simulated to account for the scattering process within the canopy. The scaling of leaf-level fluorescence emission to the canopy is based on a novel scheme for single-layer models which accounts for canopy scattering and extinction from sunlit and shaded leaves (Qiu et al., 2019). This scaling scheme is an effective approach to simulate the radiative transfer of SIF for a given canopy structure. We include two experiments similar to *BETHY-exp1/2* in the calibration of the k_N model against unstressed vs stressed species (*BEPS-exp1* and *BEPS-exp2*, respectively).

2.3.4.4 CLM4.5

The Community Land Model version 4.5 (CLM4.5) provides a description of the biogeochemical profile spanning from the sub-surface bedrock to the top of the vegetation canopy. The fluorescence sub-model follows Raczka et al. (2019), in which the degree of light saturation is calculated from the potential and actual electron transport rate as determined from the photosynthesis model described above. ϕ_f is formulated as described in Equation 2 and ϕ_P is formulated as a function of the maximum ϕ_P under dark acclimated conditions and the degree

of light saturation. CLM4.5 uses independent site-level SCOPE simulations that match the observed canopy characteristics and observed GPP at Niwot Ridge to calculate a leaf to canopy level conversion factor (κ_{740}) for estimating SIF_{canopy}. In CLM4.5, κ_{740} is fitted to the modeled SCOPE data as a function of solar zenith angle (and implicitly V_{cmax}).

Similar to Raczka et al. (2019), here we examine three separate approaches to parameterize k_N. *CLM4.5-exp1* only considers reversible NPQ (k_R), such that, $k_N = k_R$, and the relationship between k_R and the degree of light saturation is fitted to PAM fluorometry data based on Mediterranean shrubs (Flexas et al., 2002; Galmes et al., 2007). *CLM4.5-exp2* parameterizes k_R with PAM fluorometry from a Scots Pine forest (Porcar-Castell et al., 2011), and defines the rate coefficient in terms of both a reversible and sustained component ($k_N = k_R + k_S$). It has been found that sustained NPQ is important for cold climate evergreen conifer forests such as Niwot Ridge (Miguez et al., 2015; Magney et al., 2019b), and Raczka et al. (2019) found that representing both components provided improved simulations of seasonal SIF. *CLM4.5-exp3* is similar to CLM4.5-exp3 but includes a seasonally varying representation of k_R. All model experiments use hand-tuned parameters specific to US-NR1 (Raczka et al., 2016).

2.3.4.5 CLM5.0

CLM version 5.0 (CLM5.0) is similar to CLM4.5 with respect to the implementation of the fluorescence sub-model, yet includes several important updates to the representation of photosynthesis from CLM4.5, including a prognostic calculation of V_{cmax} based upon leaf nitrogen and environmental conditions, revised nitrogen limitation scheme, Medlyn stomatal conductance model, and plant hydraulic water stress (Kennedy et al., 2019). To represent NPQ we use a single approach for k_N (see *CLM4.5-exp1*), but examine three approaches for estimating κ_{740}: (1) *CLM5.0-exp1* uses κ_{740} as function of V_{cmax} following Lee et al (2015), (2) *CLM5.0-exp2* follows the approach of *CLM4.5*, and (3) *CLM5.0-exp3* adapts the approach proposed by Zeng et al. (2019) that estimates the fraction of total emitted SIF escaping the canopy by combining near-infrared reflectance of vegetation (NIR_V) and fPAR.

2.3.4.6 SIB3

The Simple Biosphere Model version 3 (SIB3) involves the use of explicit biophysical mechanisms to directly calculate carbon assimilation by photosynthesis (Baker et al., 2003; 2008). SiB3 includes prognostic calculation of temperature, moisture, and trace gases in the canopy air space, but requires prescription of most structural properties including LAI. We examine two approaches for prescribing LAI: (1) *SIB3-exp1* using values prescribed from MODIS, and (2) *SIB3-exp2* uses values observed at the study site (4.0 m^2 m^{-2}). In general, the fluorescence sub-model follows the approach of Lee et al. (2015) except that k_N is adapted to drought stressed species following van der Tol et al (2014).

2.3.4.7 SIB4

SIB4 (Haynes et al., 2019a,b) shares many similarities to SIB3 with respect to functional aspects of photosynthesis and fluorescence, however, SIB4 uses prognostic rather than prescribed phenology and LAI.

2.3.5 SCOPE

SCOPE is a multi-layer canopy model which explicitly represents the within canopy radiative transfer of fluorescence, whereas TBM-SIFs analyzed here (with the exception of BETHY) only provide an empirical representation. We provide results from a stand-alone version of SCOPE v1.73 (van der Tol et al., 2014) as an additional benchmark for TBM-SIF simulations of APAR, GPP, SIF, and quantum yields. There are three important reasons for this: (1) It is inherently difficult to provide representative and accurate *in situ* measurements of APAR, SIF, and GPP for comparison to models; (2) SCOPE provides estimates of quantum yields for fluorescence, photochemistry, and non-photochemical quenching, which are not measured continuously in the canopy at NR1; and (3) SCOPE offers a more direct benchmark for evaluating more simplified representations of canopy radiative transfer in TBM-SIFs. Unlike the TBM-SIFs, SCOPE does not include a representation of biogeochemical cycling or carbon pools, and thus no spin up is required. As such, we prescribe LAI (4 m^2 m^{-2}), canopy height (13 m), and leaf chlorophyll content (25 ug cm^{-2}) following Raczka et al. (2019). We also examine two approaches for prescribing V_{cmax}: (1) *SCOPE-exp1* uses the default constant value of 30, similar to *BETHY*, and (2) *SCOPE-exp2* uses a seasonal varying value calibrated to NR1, following Raczka et al. (2016, 2019), which follows a

bimodal distribution peaking near 45 in early summer (DOY = 150) and 40 in late summer (DOY = 250)

2.4 Data Assimilation

Details of the data assimilation protocols for ORCHIDEE is provided in Bacour et al. (2019). An ensemble of parameters related to photosynthesis (including optimal V_{cmax}) and phenology were optimized for several plant functional types. Note that none of the assimilated pixels encompass the location of the US-NR1 tower. In ORCHIDEE, the study site is treated as boreal needleleaf evergreen (ENF); as such, the *ORCHIDEE-exp3* simulations in this study are based on parameters optimized against OCO-2 SIF data using an ensemble of worldwide ENF pixels. Note that for BETHY, each experiment uses the same set of optimized parameters whereas in ORCHIDEE the SIF simulations are performed separately for the standard parameters (*ORCHIDEE-exp1/exp2*) and optimized parameters (*ORCHIDEE-exp3*), thus providing a test of sensitivity to parameter optimization as discussed below.

2.5 Illumination Conditions

In order to gain insight into how SIF emissions and quantum yields vary with illumination, we further analyze Photospec and a subset of models with respect to (a) changes in incoming light and (b) self-shading within the canopy, respectively. For PhotoSpec, we analyze changes in canopy average SIF and SIF_{rel} under conditions of predominantly direct versus diffuse PAR, using a 0.5 threshold to distinguish between the two conditions (Section 2.2.3). For models we focus on emissions from sunlit vs shaded leaves. We analyze leaf- versus canopy-level SIF emissions (SIF_{leaf} and SIF_{canopy}) in *CLM4.5-exp3*, and leaf-level quantum yields (ϕ_f, ϕ_p, ϕ_N) in *SCOPE-exp2*. We further compare predictions of quantum yield at the top-of-canopy to canopy averages in *SCOPE-exp2*. The motivation here is that top-of-canopy leaves see most of the sunlight, and thus should have different yields compared to shade adapted leaves lower in the canopy. This also provides a more direct comparison for PhotoSpec.

2.6 Modeling Protocol

Models are run for the period 2000-2018 (except BETHY (2015 only) and SCOPE (2017 only)) using identical, hourly, gap-filled meteorological observations. The primary hourly output fields

analyzed are the top-of-canopy SIF (SIF_{canopy} @ 740 nm), GPP, ϕ_f, ϕ_p, and APAR. Model-observation comparisons are made for absolute and relative SIF, GPP, SIF_{yield} (SIF_{canopy}/APAR) and GPP_{yield} (GPP/APAR), sunlit versus shaded canopies (*CLM4.5-exp3* and *SCOPE-exp2)*, and TOC versus canopy average SIF (SIF_{canopy} versus SIF_{ave}, respectively, from *SCOPE-exp2*). Quantum yields and within model experiments provide context to understand canopy integrated results. We focus our analysis on 8 am – 4 pm local time from July-August 2017 for comparison to available PhotoSpec and APAR data.

Models are controlled for meteorological forcing (meteorological data described in Burns et al., 2015) but other factors such as spin-up, land surface characteristics, parameter tuning, and model state, are not controlled for and are treated separately according to each model's protocol. For example, CLM4.5 is better suited than others in prescribing observed vegetation characteristics at the study site. One ORCHIDEE experiment (*ORCHIDEE-exp3*) is preliminary optimized by assimilating independent Orbiting Carbon Observatory 2 (OCO-2) SIF data at the global scale (Section 2.4). We emphasize that our point here is not to identify the best model but to identify common patterns in model behavior through normalized SIF and deviation from observed behavior to identify areas requiring the most attention.

The results are organized around two parallel themes. The first theme addresses four key processes driving canopy-level fluorescence: (1) incoming illumination, (2) energy partitioning on incoming light between photochemistry, fluorescence, and NPQ, and (3) leaf-to-canopy emitted SIF, including linearity of yields at leaf and canopy scale. The second theme addresses sensitivity of these processes to environmental conditions at diurnal and synoptic scales. Here, synoptic scale refers to the impact of day-to-day changes in weather, including two storm events which brought sustained cool, wet, and cloudy conditions from July 22-31 and then from August 6-10.

Section 3: Results

Incoming Illumination

Two key features dominate observed APAR variability: afternoon depression (Fig 2A) and reduction during two summer storms (Fig 2D). Both features are captured by models. More generally, models capture synoptic variability with high correlation ($r > 0.8$) and low across model

spread (σ = 10%). The exception is BETHY, which is simulated outside our observation year (2015). High model fidelity is expected given that observed PAR is prescribed, and it is promising that models show a consistent response to changes in illumination. The primary shortcoming across TBM-SIFs and SCOPE is a systematic high bias in APAR magnitude (129%), with most models exceeding the upper range of observed APAR (as determined from the six within canopy PAR sensors, Fig S2), and high model spread. These errors are likely related to differences in predicted fAPAR. In the case of ORCHIDEE, high APAR is expected due to the big leaf assumption where all leaves are considered as opaque and fully absorbing.

Canopy Photosynthesis

Observed GPP shows a broad peak from mid-morning to early afternoon (~9 am – 1 pm local), followed by slight decrease until 4 pm (Fig 2B), consistent with afternoon cooling and reduced light availability (Fig 1B-D). The two month period under investigation is relatively flat with generally weak day-to-day variability (σ = 17%), but modest correlation with APAR (r = 0.61, Fig 2E). Some models capture the afternoon GPP depression, but all models strongly underestimate its magnitude, apparently independent of stomatal conductance formulation or more explicit accounting for plant hydraulic water stress such as in CLM5.0. *SCOPE* and *BETHY*, which don't account for water stress, show no afternoon depression. Models are mostly uncorrelated with observed GPP at synoptic scale (*r* ranges from -0.2 to 0.36, highest value in SiB4), high biased, and show increased spread (in predicted magnitude) relative to APAR (143% +/- 23%). *SCOPE-exp2* shows slight improvement in GPP magnitude with the larger V_{cmax} value in late summer.

While observed GPP_{yield} is mostly stable over the diurnal cycle, most models (except BEPS) show a distinct midday minimum (Fig 3A). Half of the models show a similar midday minimum in photochemical quantum yield (ϕ_P, Fig 4A), with the other half either increasing or decreasing in the afternoon (CLM5.0 and SiB3/SiB4, respectively). The midday dip in yield is likely associated with reduced photosynthetic efficiency at high light levels, as demonstrated by reductions in GPP, GPP_{yield}, ϕ_P with APAR (Fig 5A, C, E).

Observed GPP_{yield} shows significant structure at synoptic temporal scale (Fig 3C), most notably increased yield during the cool/rainy period (reduced heat and water stress), and decreased yield

582 in mid- to late- August (increased heat and water stress following the cooling pattern). In contrast
583 to predicted GPP, models show high fidelity in capturing the magnitude and variability of GPP_{yield}
584 at synoptic scale (*r* ranges from 0.35 – 0.76, highest values in *SCOPE* and *CLM4.5/5.0*). Individual
585 models are self-consistent in their predictions of GPP_{yield} and ϕ_P at synoptic scale (r = 0.592 –
586 0.935) except for SiB3/SiB4 (r < 0.1, Fig 4B).

587 *Canopy Fluorescence*

588 Observed SIF_{canopy} is strongly correlated with observed APAR at diurnal and synoptic scale (r =
589 0.77), with common features including afternoon depression and reduction during rainy periods
590 (Fig 2C & 2F). Observed PAR also feeds into the fluorescence sub-model and, unlike GPP, strongly
591 correlates with SIF_{canopy} at synoptic scale (*r* ranges from 0.58 to 0.92, highest values in *SCOPE and*
592 *ORCHIDEE*). However, we find a persistent positive model bias in SIF_{canopy} (170% +/- 45%)
593 consistent with, but not proportional in magnitude to, the APAR bias. We note that models are
594 especially oversensitive to APAR at high light levels (Fig 5D).

595 We investigate the high bias in SIF_{canopy} in more detail using *SCOPE-exp2* and *CLM4.5-exp3*.
596 Specifically, we examine leaf and canopy level SIF and quenching under sunlit and shaded leaves.
597 Analysis of quantum yields in *SCOPE-exp2* (Fig S5) shows a reversal in the fractional amounts of
598 absorbed energy going to SIF and PQ vs NPQ in low- vs high-light conditions that is consistent
599 with leaf level data and theory (Porcar-Castell et al., 2014). More specifically, *SCOPE-exp2*
600 predicts low ϕ_F and ϕ_P and high ϕ_N in sunlit leaves relative to shaded leaves, with more energy
601 going to fluorescence and photochemistry than to NPQ in shaded leaves, and more energy going
602 to (shed off by) NPQ in sunlit leaves (Fig S5). Likewise, total ϕ_F shows decreasing values with
603 increasing APAR in *SCOPE* and *BETHY-exp2/3* compared to *BETHY-exp1*, consistent with observed
604 SIF_{yield} (Fig 5E-F), as ϕ_N ramps up to higher levels in the drought parameterized Kn model.
605 Moreover, in stark contrast to SIF_{yield} and SIF_{canopy}, ϕ_F does not show high values relative to other
606 models (Fig 4D). These results point to an issue in *SCOPE* and *BETHY* with leaf to canopy scaling
607 in needleleaf forests.

608 Analysis of *CLM4.5-exp3* suggests several possible reasons for oversensitivity to APAR. First, we
609 focus on emissions from sunlit/shaded portions of the canopy (Fig S6). *CLM4.5-exp3* and

PhotoSpec both show higher SIF under "high light" conditions (sunlit leaves and direct radiation, respectively) compared to "low light" conditions (shaded leaves and diffuse radiation, respectively), which is promising (Fig S6 A,D). Comparing the ratio of sunlit to shaded SIF in *CLM4.5-exp3* to the ratio of direct to diffuse SIF in PhotoSpec (Fig S6 B,E) shows higher ratio in *CLM4.5-exp3* on average. The difference peaks in midday, when sunlit leaf area is maximized (self-shading minimized) in CLM4.5 but no major difference in the amount of direct radiation, and decreases with increasing sun angle (morning and afternoon) and with increasing rainfall (in the afternoon on average, and during the rainy period in late July / early August), both of which increase the shaded fraction. As such, accounting for view angle and different illumination metrics for PhotoSpec and CLM4.5 (most comparable in morning, afternoon, and during rainy days) reduces, but does not entirely remove, the positive bias in high light conditions.

Second, the degree of light saturation (*x*) is twice as high in the sunlit canopy in *CLM4.5* (Fig S7), which leads to low fluorescence efficiency in sunlit leaves and high fluorescence efficiency in shaded leaves. While this produces high photochemistry in shaded leaves, it contributes a small fraction of SIF to the total canopy (~20%) despite higher fractions of shaded leaves (~2/3 at noon, Fig S6C) and thus sunlit leaves dominate SIF_{yield} and SIF_{canopy}. Therefore, it seems likely that a model's representation of canopy structure including the partitioning between sunlit/shaded leaf area fractions has an important impact upon canopy SIF. Biases in the sunlit/shaded fraction will likely propagate into the simulated value of canopy SIF. However, it's important to know that the observed sunlit/shaded fraction from PhotoSpec is estimated as well, since it is currently not possible to determine the precise sun/shade fraction within PhotoSpec FOV.

Additionally, all formulations of CLM4.5 (and most models except BETHY and SCOPE) show lack of decline in SIF_{yield} with APAR compared to measurements of absolute SIF (Fig 5E). For CLM4.5, the relationship between SIF_{yield} and APAR depends upon the relationship between degree of light saturation and reversible NPQ (Raczka et al., 2019). This suggests it is important to properly represent the NPQ response to environmental conditions when simulating SIF.

While most of the model bias is reduced in SIF_{yield} (126%, mostly attributed to BETHY and SCOPE), the remaining signal, representing the dynamic response to synoptic conditions (e.g., Magney et al., 2019), is poorly represented in models, as demonstrated in a time series of 5-day means (Fig

3D). Most models show zero to strongly negative correlation with observations at synoptic scale and only three models (*SCOPE*, *ORCHIDEE-exp3,* and *BETHY-exp2/3)*, produce correlation greater than 0.5. These are the only three models that also capture a negative relationship between SIF_{yield} and APAR (Fig 5E).

In general, predicted SIF_{yield} is stable during our short study period (Fig 3). Half of models show a significant positive correlation with GPP_{yield} ($r > 0.85$) and half show zero or negative correlation (Fig S8). While these findings run counter to observed SIF_{yield}, which shows a clear response during and following the storm event and moderate positive correlation with observed GPP_{yield} ($r = 0.40$), they show some consistency with observed SIF_{rel} (grey line in Fig 3 and Fig S8A) which like many models is stable and uncorrelated with GPP_{yield}. We refer the reader to Section 2.2.2 for clarification of the important difference between SIF_{yield} and SIF_{rel}.

Leaf-to-Canopy Scaling

Several methods have been proposed to transfer predicted leaf-level SIF emissions to the top of canopy. While leaf-to-canopy scaling enables efficient global scale simulation, the diversity of novel methods adds uncertainty to the canopy level estimate of SIF (in addition to aforementioned uncertainties in structure, APAR, photochemistry, fluorescence). These differences are evident in comparison of Figures 3 and 4, in which yields are plotted on a similar scale.

At least at diurnal scale, there is some evidence that leaf and canopy emissions look more similar for models adopting simplified empirical scaling functions (SiB3, SiB4, CLM4.5, CLM5.0, BEPS) than for models that more explicitly account for radiative transfer (SCOPE, BETHY, ORCHIDEE). For the more explicit models, the diurnal cycle of ϕ_f is out of phase with SIF_{yield}, the former of which peaks in the afternoon and the latter of which peaks in the morning. This produces reasonable agreement to PhotoSpec in phase and magnitude between SIF_{yield} and SIF_{rel} for ORCHIDEE, but produces divergence in the magnitude of SIF_{canopy} for ORCHIDEE.

Model performance in leaf-to-canopy scaling is summarized in Figure S8. The only three models with a positive relationship between yields (Fig S8B) and between quenching terms (Fig S8C) include explicit representation of radiative transfer (i.e., SCOPE, BETHY, and ORCHIDEE). CLM4.5

667 is the only model with a positive relationship between yields, but not between quenching terms.
668 SiB3/SiB4 are the only models with a positive relationship between quenching terms, but not
669 between yields.

670 Finally, we clarify an important difference between observed and predicted estimates of canopy
671 average SIF. PhotoSpec scans direct emissions from sunlit and shaded leaves within the canopy,
672 thus observing the 'total' emission from leaves in the instrument FOV. We then average each of
673 these leaf-level scans and report as canopy averages. Model output, in contrast, is reported at
674 the TOC, which represents the 'net' emission from leaves after attenuation in the canopy
675 (through canopy radiative transfer, re-absorption of SIF, and shading). Assuming sunlit and
676 shaded leaves within the canopy emit at the same rate as TOC leaves, attenuation will reduce the
677 effective signal from leaf-level emissions within the canopy. As such, the average of leaf level
678 emissions (canopy average) is expected to be lower than the net emission of leaves reaching the
679 top of canopy.

680 This is important because CLM4.5 shows strong attenuation of SIF from leaf-level to TOC,
681 decreasing by a factor of 2-3 at midday (Fig S7). The interpretation here is that the model bias in
682 absolute SIF may actually be higher than reported here; however, we note that more quantitative
683 information on the observed fraction of sunlit vs shaded leaves and comparative top-of-canopy
684 SIF values for the same canopy elements are needed (to account for off-nadir SIF viewing) for
685 more accurate determination of scaling between observed canopy and top-of-canopy SIF.

686 *Within Model Experiments*

687 In most cases, within model experiments produce improvements in some metrics and
688 degradation across others (performance change is quantified by reporting correlation values in
689 brackets). An important and unexpected result of this study is the impact of different levels of
690 tuning to observations on our predictions. While this work represents a snapshot of the state-of-
691 the-art in site-level TBM-SIF modeling, and we have taken great care to control for environmental
692 conditions (most important being illumination), an important overall takeaway is for future
693 model comparisons to make additional efforts to control for initial conditions and vegetation
694 state (i.e. model biophysical parameters).

695 The most basic example is tuning of LAI in SiB3 and V_{cmax} in SCOPE. LAI, as prescribed by MODIS
696 for *SiB3-exp1* (~1.5), is on the low end for a subalpine evergreen forest, and consequently
697 produces negative biases in APAR, GPP, SIF and SIF_{yield}. When prescribed according to tower
698 observations in *SiB3-exp2* (~4.0), the biases become positive (albeit on the lower end of the
699 model ensemble), but produces degraded variation at synoptic scale for GPP (0.39 vs 0.19), SIF
700 (0.87 vs .71) and SIF_{yield} (0.09 vs -0.32). The tuning of V_{cmax} in SCOPE improves the magnitude of
701 GPP, with minimal impact on variability at diurnal- to synoptic- scale.

702 Experiments in CLM4.5 comprise a higher level of hand tuning of vegetation structural and
703 functional characteristics. Parameter tuning was imposed to match vegetation structure with
704 site level measurements and consequently CLM4.5 produces overall low bias in yields. With
705 respect to synoptic variation, NPQ experiments, tuned against the measured air temperature and
706 a representative evergreen forest, produce improvements at synoptic scale for GPP (-0.01 vs
707 0.16), SIF (0.59 vs 0.86), and GPP_{yield} (0.05 vs 0.63), but degradation in SIF_{yield} (0.32 vs -0.25).
708 Likewise, NPQ experiments in BETHY based on species information (calibration of K_N against PAM
709 fluorescence in stressed vs unstressed systems) shows improvement in the SIF_{yield}-APAR
710 relationship for drought stressed models (*BETHY-exp1* vs *BETHY-exp2/3*).

711 Experiments with ORCHIDEE demonstrate that errors in model parameters (such as V_{cmax}, LAI_{max},
712 leaf age, or SLA) contribute to SIF and GPP uncertainty but can be alleviated by assimilation of
713 OCO-2 SIF retrievals (*ORCH-exp1/2* vs *ORCH-exp3*). Model optimization of parameters improves
714 the functional link between SIF and GPP, thus reducing biases in APAR, GPP, and SIF_{yield}, and
715 improving synoptic variation in SIF_{yield} (-0.04 vs 0.58).

716 **Section 4. Discussion**

717 This study represents a first attempt to evaluate a controlled ensemble of TBM-SIF models
718 against canopy integrated SIF observations to identify and attribute model-observation
719 mismatches related to errors in canopy absorption of sunlight, photosynthesis, fluorescence, and
720 leaf-to-canopy radiative transfer of fluorescence.

721 Different models match some observed parameters better than others (with respect to APAR and
722 yield), but no model gets both APAR and SIF_{yield} magnitude and/or sensitivities close to the

observations. For example, BEPS closely matches the magnitude of APAR (Fig 2A), and BETHY captures the decline in SIF_{yield} with APAR for NPQ quenching based on stressed species (Fig 5E), but both models overestimate observed yield by a factor of 2, hence SIF is overestimated (Fig 2). CLM4.5 correctly captures the diurnal SIF_{yield} change, but overestimate APAR; in this case, SIF and SIF_{yield} are overestimated. Importantly, models diverge strongly from each other and from observations in the magnitude of SIF_{yield} and its decline with APAR (Fig 5E), partially reflecting model variability in ϕ_f (Fig 5F), but in general show a characteristic pattern of weak SIF_{yield} decline with APAR. GPP_{yield} shows higher agreement between models and with observations (Fig 5B), despite divergent ϕ_P (Fig 5C), which could be indication that the primary uncertainty is due to the representation of fluorescence and not the photosynthesis model.

Consequently, we find a strong linear and positive relationship between observed SIF_{yield} and GPP_{yield} for absolute SIF, which is underestimated on average by models (Fig S8A-B). In contrast, models show quite strong positive relationships between ϕ_f and ϕ_P (Fig S8C). Our study highlights an apparent challenge for models in transferring leaf level processes to canopy scale, and consequently, linking the proper canopy mechanistic SIF-GPP relationship at the leaf level.

The mismatch between multi-model simulations and tower-based observations of SIF and GPP at hourly and daily scales can be summarized as symptoms of five main factors: (1) PhotoSpec scan strategy, (2) radiative transfer of incoming PAR and impact on APAR and sunlit/shaded fraction, (3) representation of photosynthesis and sensitivity to water limitation especially during afternoon conditions, (4) representation of fluorescence and sensitivity to reversible NPQ response at Niwot Ridge, and (5) radiative transfer of fluorescence from leaf to canopy. Several persistent biases falling under these broad categories are discussed below.

Apples to Apples Comparison.

PhotoSpec is unique in its ability to scan entire canopies for signals that are largely hidden from nadir-oriented instruments. However, this creates unique challenges for interpretation of data and comparison to models. For example, the diurnal cycle of observed SIF is highly sensitive to view angle. PhotoSpec was set up in 2017 to scan back-and-forth between northwest and northeast view angles, but the instrument was slightly biased to the northwest, causing a low

751 phase angle in the morning (more aligned with rising sun) and increased phase angle in the
752 afternoon (more opposed to setting sun). As such, PhotoSpec observed predominantly
753 illuminated canopies in the morning and shaded canopies in the afternoon (i.e., more shaded
754 fraction), leading to the late morning peak in reflected radiance (Fig S3).

755 Moreover, Photospec scans specific locations at the top of the canopy from near nadir to view
756 angles closer to the horizon (see Fig. S8 in Magney et al., 2019b), while models are currently
757 configured to simulate top of canopy emission and simulated here as nadir viewing. The question
758 becomes whether to retain nadir only data and sacrifice signal-to-noise, or to average over all
759 elevation angles and risk aliasing view angle effects. This study, partly motivated by high
760 agreement of canopy integrated SIF with spaceborne data from OCO-2 and TROPOMI (Magney
761 et al., 2019b; Parazoo et al., 2019), has chosen the latter approach but with an attempt to
762 minimize scan angle effects in SIF_{rel}. However, it is worth noting that swath sensors such as
763 GOME-2 show high sensitivity to viewing angle especially under increasing illumination angles
764 (Kohler et al., 2018; Joiner et al., in review). View angle effects are likely to be especially acute
765 for PhotoSpec in the morning and afternoon with increasing anisotropy and changes in the
766 illuminated field of view with sun and view angle. Other tower SIF instruments with a wide FOV
767 (i.e. FluoSpec2; Yang et al., 2018) may more appropriately represent the TOC SIF emission, but
768 also have difficulty disentangling the sunlit/shaded canopy components.

769 It is critical that model evaluation relative to measured SIF data and data assimilation studies
770 properly account for the specificities of the instrument (viewing of the instrument, spectral band,
771 time of the overpass for space-borne instruments), the representation of canopy emission, and
772 correct observations for directional variations in SIF relative to observation geometry. Although
773 normalizing SIF by reflected radiance partially alleviates scan angle effects, this highlights the
774 need for models to get canopy structure, radiative transfer, and sunlit/shaded fraction correct,
775 which feed all the way through to SIF and GPP. Further ground-based investigations of SIF
776 anisotropy, sunlit/shade fraction, and vertical distribution (within canopy, canopy integrated,
777 and top of canopy) with PhotoSpec and SCOPE may help to inform models on the physical aspects
778 of the signal. Despite the issues we highlight in comparing observations to models, the potentially

more interesting and important story here is with respect to model-model comparisons, which reveals wide divergence in response to light conditions and other factors, as discussed below.

TBM SIF is too sensitive to APAR.

Our results indicate a wide range of SIF responses to APAR: TBM-SIFs and SCOPE are usually far too sensitive to APAR, observations of absolute SIF are less sensitive, and observations of relative SIF (SIF_{rel}) are least sensitive (Fig. 5D). We remind the reader that SIF_{rel} is normalized by the amount of far-red light reflected from leaves in the FOV of PhotoSpec, and thus has reduced sensitivity to absorbed light than absolute SIF. The fact that SIF_{rel} is the least sensitive to APAR means other processes are driving changes in SIF under increased light absorption. In this case, it reveals a strong SIF response to changes in photochemical quenching. SIF models appear especially sensitive to sunlit leaves. In CLM4.5, SIF emissions from the sunlit portion of the canopy are a factor of 5 higher than emissions from shaded leaves, despite twice as fewer leaves in the sunlit canopy (Fig S6C). In CLM4.5, the combination of higher than average ϕ_f (Fig 5F) with higher fluorescence efficiency in the sunlit portion of the canopy, produce an increase in the magnitude and sensitivity to sunlit fraction, thus contributing to the high bias (factor of 3 higher than observed) and strong diurnal cycle (2-fold increase from morning to midday).

Linearity of SIF and GPP yields.

Observations show a positive but not significant linear relationship between SIF_{yield} and GPP_{yield} (Fig 8A, r = 0.40) at our study site. This is likely due to the short time period investigated here where there is relatively little change in SIF_{yield} and GPP_{yield} during peak summer. Half of models (4 of 8) show a significant (r > 0.35) linear and positive slope (r > 0.35; SCOPE, ORCH-exp3, CLM4.5-exp3, and BETHY-exp3) between SIF_{yield} and GPP_{yield}, while 6 models (except CLM5.0) show a significant positive slope between quantum yields (ϕ_f and ϕ_p, Fig S8C). These regression plots of quantum yields, in turn, help explain the observed linearity of SIF_{yield} vs. GPP_{yield}: At least in the case of Niwot Ridge, model (and presumably observed) ϕ_p stays within high light "NPQ-Phase" conditions, and generally doesn't exceed the range in which decoupling of ϕ_f and ϕ_p (ϕ_p > 0.6) in low light "PQ-Phase' conditions occurs (Porcar-Castell et al., 2014, cf Fig 9). SCOPE and BETHY-exp3, which best capture the observed relationship in the canopy between SIF_{yield} and

807 GPP_{yield}, are also the only models that also show a decline in SIF_{yield} with APAR, as discussed below.
808 These results are likely to change when we expand the study to several years; however, the
809 purpose of this study was to provide an initial investigation into the response of modelled SIF and
810 GPP to light during peak summer.

811 **Insufficient decline in SIF_{yield} with APAR.**

812 In general, models show an insufficient decline in SIF_{yield} with APAR, when compared to observed
813 SIF_{yield} (Fig 5E). All models except SiB3 and SiB4 show some decline, with BETHY showing the best
814 agreement in slope magnitude. SCOPE and BETHY are the only models with full radiative transfer
815 but this does not appear to have a substantial impact on SIF_{yield}, which has a similar (albeit
816 suppressed) decline with APAR as ϕ_f (Fig 5F). Within model experiments show little to no
817 sensitivity of SIF_{yield} or ϕ_f decline with APAR to water stress (e.g., ORCHIDEE) or prescribed LAI
818 (e.g., SiB3), but high sensitivity to the formulation of NPQ with respect to species calibration (e.g.,
819 BETHY) and reversibility (e.g., CLM4.5).

820 Three CLM4.5 experiments demonstrate sensitivity to representation of NPQ variability at diurnal
821 and seasonal scales. The first simulation using the default NPQ parameterization from SCOPE
822 (*CLM4.5-exp1*, based on a 2-parameter fit to drought stressed Mediterranean species (Galmes et
823 al., 2007) produces the strongest decline in SIF_{yield}. The second simulation, which includes a site-
824 specific NPQ formulation that accounts for k_R and k_S (*CLM4.5-exp2*), produces the weakest
825 decline. The third simulation with seasonally varying k_R produces a slightly stronger decline. An
826 important point for this formulation is that k_R is constrained by PAM fluorometry data at Hyytiala
827 (Scot Pine) and does not account for high light saturation values and summer drought conditions
828 that may be more typical of lower latitude sites such as Niwot Ridge. This could indicate that
829 parameterizing k_R based upon similar PFTs may not be sufficient to properly characterize the NPQ
830 response for lower latitude sites such as Niwot Ridge.

831 Similar results are found in experiments with BETHY comparing stressed (drought) and
832 unstressed (relative to water availability) NPQ models at NR1 but controlling for k_R (constant in
833 time in both cases, stronger negative SIF_{yield} response to APAR in stressed model). In the
834 unstressed models of CLM4.5 and BETHY, the NPQ response to APAR becomes too low, causing

an oversensitivity of SIF to APAR and thus high SIF bias. The strongly regulated NPQ response of the drought-based model enables more non-photochemical quenching at high light levels in stressed ecosystems compared to typical unstressed plants. While this k_{NPQ} model was developed using drought-stressed plants, similar up-regulation of NPQ is expected to occur under any condition where photosynthesis is limited and available excitation energy is high (e.g. cold temperatures and high light, Sveshnikov et al., 2006). Our results thus emphasize the need for careful implementation of NPQ dynamics for simulating and assimilating SIF in different light and stress environments (Raczka et al., 2019; Norton et al., 2019).

Data assimilation reduces high bias. Assimilation of OCO-2 SIF in ORCHIDEE brings the magnitude of both GPP and SIF in closer agreement with observations. This improvement is driven by decreases in leaf photosynthetic capacity (V_{cmax}, LAI_{max}, leaf age, SLA, Bacour et al., 2019), which decreases the magnitude (but not shape) of APAR closer to observed values (Fig 2), and leads to improvements in GPP_{yield} and SIF_{yield} (Fig 3). Nevertheless, after the assimilation there are still disagreements in SIF_{yield} vs GPP_{yield} relative to the measured quantities (Fig S8). For diurnal and synoptic cycles, the assimilation effectively acts to scale the magnitude of SIF, GPP and APAR (and related yields), but it does little to alter variability. Although data assimilation (i.e. calibrating model parameters) is critical to improving modelled SIF and GPP, this should be done in conjunction with improvements in the model formulation (as summarized in Section 5), otherwise the estimated model parameters can be sub-optimal to compensate for the lack of missing processes.

5. Conclusions/Recommendations

Our results reveal systematic biases across TBM-SIF models affecting leaf-to-canopy simulations of APAR, GPP, and SIF. This highlights key areas where observing strategies and model formulations can be improved:

1) Radiative transfer of incoming and absorbed PAR. The representation of incoming radiative transfer produces positive biases in APAR that leads to positive biases in GPP, both of which occur regardless of time of day. This is influenced by characterization of the canopy, leaf orientation and clumping, biochemical content, canopy layers, and leaf area, which dictates

the sunlit/shaded fractions of the canopy. Furthermore, the combination of high APAR bias in models and high uncertainty in observed APAR highlights a need for more accurate and representative *in situ* measurements of APAR within the FOV of SIF observations and footprint of eddy covariance data. We recommend further site-level investigation of observed and simulated canopy light absorption, emphasizing comparison of multi-layer and multi-leaf radiation schemes accounting for sunlit and shaded leaf area.

2) Water stress impacts on photosynthesis. The underlying photosynthetic models fail to simulate the magnitude of depression of observed GPP in the afternoon, regardless of how stomatal-conductance and water stress models and parameters are formulated. This likely results from the inability to account for afternoon water stress to properly restrict stomatal conductance and hence GPP and SIF. Additional effort is needed to characterize SIF and GPP sensitivity to increased atmospheric demand and/or reduced soil moisture across a range of managed and unmanaged systems. We also recommend more inclusion of stomatal optimization models (e.g., Eller et al., 2020) as optional parameterizations for TBMs, to better account for plant hydraulic functioning under water stress compared to the more widely used semi-empirical models.

3) Leaf Mechanism for Energy Partitioning. We provide evidence that many models fail to capture the correct reversible NPQ response to light saturation, leading to biases in SIF_{yield} during high light conditions and especially with increasing moisture limitation at the end of summer. Further investigation using models such as BETHY and CLM is needed to better characterize sensitivity of NPQ formulations to PFT and environmental conditions. We also emphasize a need for more simultaneous measurements of active and passive chlorophyll fluorescence to determine the temporal dynamics of competing pathways (PQ, NPQ) from a wider variety of plant species under ambient conditions and different levels of stress.

4) Radiative transfer of SIF. SIF is emitted from the leaf level and then is transferred to the top of canopy as a function of canopy structure (leaf geometry, canopy layers, leaf area, sunlit/shaded fraction). Despite high disagreement of SCOPE and BETHY with respect to the simulation of APAR and SIF magnitude, we recommend site level simulations using a similar

framework where a radiative transfer model is run both offline and coupled to a terrestrial biosphere model for more detailed investigation of sensitivity to canopy characteristics.

5) Observation strategy. The PhotoSpec scan strategy enables direct measurement of SIF emission at leaf-to-canopy scale, but requires off-nadir view angles that lead to changing fractions of sunlit and shaded canopies throughout the day as a function of sun angle. Further work could be done using tower mounted instruments with a wider FOV that more accurately represent top of canopy emissions for comparison to model simulations, and to classify emissions from shaded vs sunlit canopies. More effort is also needed to better align models with observations, for example by leveraging three-dimensional capabilities in SCOPE (and other RTMs) to directly account for multiple observation angles.

6) Finally, we note that our focus on a water limited subalpine evergreen needleleaf forest represents a challenging case study for models and observations. In many cases, there is strong covariance between LAI, SIF, APAR and GPP in cropping systems (Dechant et al., 2020), but because this study site experiences little change in canopy structure and APAR throughout the season (Magney et al, 2019b), our study sought to provide more explicit insight into the models sensitivity to photosynthesis and fluorescence. As such, it is possible that we would see more convergence of results, and a reduction in confounding effects (e.g., decreased NPQ), in a well-watered high-LAI cropping system. We therefore recommend similar model-observation assessments across a wider range of biota and climate.

Data availability

All observational data (APAR, SIF, GPP, and relative SIF) are provided as hourly time series. The data can be found at https://data.caltech.edu/records/1231. The data are saved as a .csv file.

Author Contribution

NP, TM, and IB designed research. NP, TM, AN, BR, CB, FM, IB, YZ, BQ, MS, DB performed research; AN, BR, CB, FM, IB, YZ, BQ, MS, NM contributed model simulations; TM, DB, SP, PB, JS, KG, CF contributed observational data; NP, TM, AN, BR analyzed data; NP, TM, AN, BR, CB, IB, YZ, NM, DB, CF wrote paper.

Competing Interests

The authors declare that they have no conflict of interest.

Acknowledgements

The US-NR1 AmeriFlux site is supported by the U.S. DOE, Office of Science through the AmeriFlux Management Project (AMP) at Lawrence Berkeley National Laboratory under Award Number 7094866. BMR was supported by the NASA CMS Project (award NNX16AP33G) and the US Department of Energy's Office of Science, Terrestrial Ecosystem Science Program (awards DE-SC0010624 and DE-SC0010625). CESM (CLM4.5 and CLM5.0) is sponsored by the National Science Foundation and the U.S. Department of Energy. ORCHIDEE is supported by CNES-TOSCA under the FluOR and ECOFLUO projects. ITB was supported by NASA contract 80NSSC18K1312. We would like to thank the W.M. Keck Institute for Space Studies and internal funds from the Jet Propulsion Laboratory for support of the field measurements at Niwot Ridge (http://www.kiss.caltech.edu/study/photosynthesis/technology.html). A portion of this research was carried out through the OCO-2 project at the Jet Propulsion Laboratory, California Institute of Technology, under contract with NASA. This work was supported in part by the NASA Earth Science Division MEaSUREs program (grant 17-MEASURES-0032) and ABoVE program (18-TE18-0062).

References

Aasen, H., Van Wittenberghe, S., Medina, N. S., Damm, A., Goulas, Y., Wieneke, S., Hueni, A., Malenovsky, Z., Alonso, L, Pacheco-Labrador, J., and Cendrero-Mateo, M.P.: Sun-induced chlorophyll fluorescence II: Review of passive measurement setups, protocols, and their application at the leaf to canopy level. *Remote Sensing*, *11*(8), p.927, 2019.

Anav, A., Friedlingstein, P., Beer, C., Ciais, P., Harper, A., Jones, C., Murray-Tortarola, G., Papale, D., Parazoo, N.C., Peylin, P., and Piao, S.: Spatiotemporal patterns of terrestrial gross primary production: A review, Reviews of Geophysics, 53(3), 785-818, https://doi.org/10.1002/2015RG000483, 2015.

Albert, L. P., Keenan, T. F., Burns, S. P., Huxman, T. E., and Monson, R. K.: Climate controls over ecosystem metabolism: insights from a fifteen-year inductive artificial neural network synthesis for a subalpine forest, Oecologia, 184(1), 25–41. https://doi.org/10.1007/s00442-017-3853-0, 2017

Bacour, C., Maignan, F., MacBean, N., Porcar-Castell, A., Flexas, J., Frankenberg, C., Peylin, P., Chevallier, F., Vuichard, N., and Bastrikov, V.: Improving estimates of Gross Primary Productivity by assimilating solar-induced fluorescence satellite retrievals in a terrestrial biosphere model using a process-based SIF model, Journal of Geophysical Research: Biogeosciences, 124(11), 3281-3306, 2019.

Baker, I.T., Prihodko, L., Denning, A.S., Goulden, M., Millller, S., and da Rocha, H.: Seasonal Drought Stress in the Amazon: Reconciling Models and Observations, J.Geophys. Res., 113, G00B01, doi:10.1029/2007JG000644, 2008.

Baker, I.T., A.S. Denning, N. Hanan, L. Prihodko, P.-L. Vidale, K. Davis and P. Bakwin: Simulated and observed fluxes of sensible and latent heat and CO2 at the WLEF-TV Tower using SiB2.5, Glob. Change Biol., 9, 1262-1277, 2003.

Ball, J. T., Woodrow, I. E., and Berry, J. A.: A model predicting stomatal conductance and its contribution to the control of photosynthesis under different environmental conditions, Progress in photosynthesis research, Springer, Dordrecht, 221-224, 1987.

Burns, S. P., Blanken, P. D., Turnipseed, A. A., Hu, J., and Monson, R. K.: The influence of warm-season precipitation on the diel cycle of the surface energy balance and carbon dioxide at a Colorado subalpine forest site, Biogeosciences, 12, 7349–7377, 2015.

Burns, S. P., Swenson, S. C., Wieder, W. R., Lawrence, D. M., Bonan, G. B., Knowles, J. F., and Blanken, P. D.: A comparison of the diel cycle of modeled and measured latent heat flux during the warm season in a Colorado subalpine forest, Journal of Advances in Modeling Earth Systems, 10, 617–651, 2018.

970 Chen, J. M., Liu, J., Cihlar, J., and Goulden, M. L.: Daily canopy photosynthesis model through
971 temporal and spatial scaling for remote sensing applications, Ecological Modelling, 124(2–
972 3), 99–119, 1999.

973 Demmig-Adams, B., Cohu, C. M., Muller, O., and Adams, W. W.: Modulation of photosynthetic
974 energy conversion efficiency in nature: from seconds to seasons, Photosynthesis Research,
975 113(1–3), 75–88. https://doi.org/10.1007/s11120-012-9761-6, 2012.

976 Dechant, B., Ryu, Y., Badgley, G., Zeng, Y., Berry, J.A., Zhang, Y., Goulas, Y., Li, Z., Zhang, Q.,
977 Kang, M., Li, J., Moya, I.: Canopy structure explains the relationship between
978 photosynthesis and sun-induced chlorophyll fluorescence in crops, Remote Sensing of
979 Environment, 241, 111733, 2020.

980 Dufresne, J.-L., Foujols, M.-A., Denvil, S., Caubel, A., Marti, O., Aumont, O., Balkanski, Y., Bekki,
981 S., Bellenger, H., Benshila, R., and Bony, S.: Climate change projections using the IPSL-CM5
982 Earth System Model: from CMIP3 to CMIP5, Climate Dynamics, 40(9–10), 2123–2165,
983 2013.

984 Eller, Cleiton B., Rowland, L., Mencuccini, M., Rosas, T., Williams, K., Harper, A., Medlyn, B. E.,
985 Wagner, Y., Klein, T., Teodoro, G.S. and Oliveira, R.S.: Stomatal optimisation based on
986 xylem hydraulics (SOX) improves land surface model simulation of vegetation responses to
987 climate, *New Phytologist*, 2020.

988 Flexas, J., Escalona, J. M., Evain, S., Gulías, J., Moya, I., Osmond, C. B., and Medrano, H.: Steady-
989 state chlorophyll fluorescence (Fs) measurements as a tool to follow variations of net CO2
990 assimilation and stomatal conductance during water-stress in C3 plants. Physiologia
991 Plantarum, 114(2), 231–240. https://doi.org/10.1034/j.1399-3054.2002.1140209.x, 2002.

992 Friedlingstein, P., Meinshausen, M., Arora, V. K., Jones, C. D., Anav, A., Liddicoat, S. K., and
993 Knutti, R.: Uncertainties in CMIP5 climate projections due to carbon cycle feedbacks,
994 Journal of Climate, 27(2), 511–526, 2014.

995 Galmés, J., Flexas, J., Savé, R., and Medrano, H.: Water relations and stomatal characteristics of
996 Mediterranean plants with different growth forms and leaf habits: responses to water
997 stress and recovery, Plant and Soil, 290(1–2), 139–155, 2007.

998 Gastellu-Etchegorry, J. P., Malenovský, Z., Duran Gomez, N., Meynier, J., Lauret, N., Yin, T., Qi,
999 J., Guilleux, J., Chavanon, E., Cook, B., Morton, D.: Simulation of chlorophyll fluorescence
1000 for sun- and shade-adapted leaves of 3D canopies with the DART model, International
1001 Geoscience and Remote Sensing Symposium (IGARSS), 2018-July, 5995–5998.
1002 https://doi.org/10.1109/IGARSS.2018.8517576, 2018.

1003 Grossmann, K., Frankenberg, C., Magney, T. S., Hurlock, S. C., Seibt, U., and Stutz, J.: PhotoSpec:
1004 A new instrument to measure spatially distributed red and far-red Solar-Induced
1005 Chlorophyll Fluorescence, Remote Sensing of Environment, 216, 311–327.
1006 https://doi.org/10.1016/j.rse.2018.07.002, 2018.

1007 Gu, L., Han, J., Wood, J. D., Chang, C. Y., and Sun, Y.: Sun-induced Chl fluorescence and its
1008 importance for biophysical modeling of photosynthesis based on light reactions, New
1009 Phytologist, nph.15796. https://doi.org/10.1111/nph.15796, 2019.

1010 Gu, L., Wood, J. D., Chang, C. Y. Y., Sun, Y., and Riggs, J. S.: Advancing Terrestrial Ecosystem
1011 Science With a Novel Automated Measurement System for Sun-Induced Chlorophyll
1012 Fluorescence for Integration With Eddy Covariance Flux Networks, Journal of Geophysical
1013 Research: Biogeosciences, 124(1), 127–146. https://doi.org/10.1029/2018JG004742, 2019.

1014 Haynes, K., Baker, I. T., Denning, S., Stöckli, R., Schaefer, K., Lokupitiya, E. Y., and Haynes, J. M.:
1015 Representing grasslands using dynamic prognostic phenology based on biological growth
1016 stages: 1. Implementation in the Simple Biosphere Model (SiB4), Journal of Advances in
1017 Modeling Earth Systems, 11. https://doi.org/10.1029/ 2018MS001540, 2019a.

1018 Haynes, K. D., Baker, I. T., Denning, A. S., Wolf, S., Wohlfahrt, G., Kiely, G., Minaya, R. C., and
1019 Haynes, J. M.: Representing grasslands using dynamic prognostic phenology based on
1020 biological growth stages: 2. Carbon cycling, Journal of Advances in Modeling Earth
1021 Systems, 11. https:// doi.org/10.1029/2018MS001541, 2019b.

1022 Julitta, T., Burkart, A., Colombo, R., Rossini, M., Schickling, A., Migliavacca, M., Cogliati, S.,
1023 Wutzler, T., Rascher, U.: Accurate measurements of fluorescence in the O2A and O2B band
1024 using the FloX spectroscopy system - results and prospects. In: Proc. Potsdam GHG Flux
1025 Workshop: From Photosystems to Ecosystems, 24–26 October 2017, Potsdam, Germany.
1026 https://www.potsdam-flux-workshop.eu/, 2017

1027 Kaminski, T., Knorr, W., Schürmann, G., Scholze, M., Rayner, P. J., Zaehle, S., Blessing, S., Dorigo,
1028 W., Gayler, V., Giering, R., and Gobron, N.: The BETHY/JSBACH carbon cycle data
1029 assimilation system: Experiences and challenges, Journal of Geophysical Research:
1030 Biogeosciences, 118(4), 1414–1426, 2013.

1031 Kennedy, D., Swenson, S., Oleson, K. W., Lawrence, D. M., Fisher, R., Lola da Costa, A. C., and
1032 Gentine, P.: Implementing plant hydraulics in the community land model, version
1033 5, Journal of Advances in Modeling Earth Systems, 11(2), 485-513, 2019.

1034 Koffi, E. N., Rayner, P. J., Scholze, M., and Beer, C.: Atmospheric constraints on gross primary
1035 productivity and net ecosystem productivity: Results from a carbon-cycle data assimilation
1036 system, Global Biogeochemical Cycles, 26(1), https://doi.org/10.1029/2010GB003900,
1037 2012.

1038 Koffi, E. N., Rayner, P. J., Norton, A. J., Frankenberg, C., and Scholze, M.: Investigating the
1039 usefulness of satellite-derived fluorescence data in inferring gross primary productivity
1040 within the carbon cycle data assimilation system, Biogeosciences, 12(13), 4067–4084,
1041 2015.

Krinner, G., Viovy, N., de Noblet-Ducoudré, N., Ogée, J., Polcher, J., Friedlingstein, P., Ciais, P., Sitch, S., and Prentice, I. C.: A dynamic global vegetation model for studies of the coupled atmosphere-biosphere system, Global Biogeochemical Cycles, 19(1), 2005.

Lee, J.-E., Berry, J. A., van der Tol, C., Yang, X., Guanter, L., Damm, A., Baker, I., and Frankenberg, C.: Simulations of chlorophyll fluorescence incorporated into the Community Land Model version 4, Global change biology, 21 (9), 3469-3477, 2015.

Leuning R.: A critical appraisal of a combined stomatal-photosynthesis model for C_3 plants, Plant Cell Environ, **18**: 339–357, 1995.

Li, Z., Zhang, Q., Li, J., Yang, X., Wu, Y., Zhang, Z., Wang, S., Wang, H., and Zhang, Y.: Solar-induced chlorophyll fluorescence and its link to canopy photosynthesis in maize from continuous ground measurements, Remote Sensing of Environment, 236, 111420, 2020.

Liu, J., Chen, J. M., and Cihlar, J.: Mapping evapotranspiration based on remote sensing: An application to Canada's landmass, Water Resources Research, 39(7), 2003.

Liu, W., Atherton, J., Mõttus, M., Gastellu-Etchegorry, J. P., Malenovský, Z., Raumonen, P., et al.: Simulating solar-induced chlorophyll fluorescence in a boreal forest stand reconstructed from terrestrial laser scanning measurements, Remote Sensing of Environment, (July 2018), 111274, https://doi.org/10.1016/j.rse.2019.111274, 2019.

Medlyn, B.E., Duursma, R.A., Eamus, D., Ellsworth, D.S., Prentice, I.C., Barton, C.V.M., Crous, K.Y., De Angelis, P., Freeman, M., and Wingate, L.: Reconciling the optimal and empirical approaches to modelling stomatal conductance, Global Change Biology, 17: 2134–2144. doi:10.1111/j.1365-2486.2010.02375.x, 2011.

Magney, T. S., Frankenberg, C., Fisher, J. B., Sun, Y., North, G. B., and Davis, T. S.: Connecting active to passive fluorescence with photosynthesis : a method for evaluating remote sensing measurements of Chl fluorescence, New Phytologist, 215(4), 1594-1608, https://doi.org/10.1111/nph.14662, 2017.

Magney, T. S., Frankenberg, C., Köhler, P., North, G., Davis, T. S., Dold, C., Dutta, D., Fisher, J. B., Grossmann, K., Harrington, A., Hatfield, J.: Disentangling Changes in the Spectral Shape of Chlorophyll Fluorescence: Implications for Remote Sensing of Photosynthesis, Journal of Geophysical Research: Biogeosciences, 124(6), 1491-1507, https://doi.org/10.1029/2019JG005029, 2019a.

Magney, T. S., Bowling, D. R., Logan, B., Grossmann, K., Stutz, J., and Blanken, P.: Mechanistic evidence for tracking the seasonality of photosynthesis with solar-induced fluorescence, Proceedings of the National Academy of Sciences, 116 (24), 11640-11645, https://doi.org/10.1073/pnas.1900278116, 2019b.

Magney, T., Frankenberg, C., Grossmann, K., Bowling, D., Logan, B., Burns, S., and Stutz, J.: Canopy and needle scale fluorescence data from Niwot Ridge, Colorado 2017-2018 (Version 1.1) [Data set]. CaltechDATA. https://doi.org/10.22002/d1.1231. 2019c.

Miguez, F., Fernández-Marin, B., Becerril, J. M., and Garcia-Plazaola, J. I.: Activation of photoprotective winter photoinhibition in plants from different environments: a literature compilation and meta-analysis, Physiologia Plantarum, 155(4), 414–423, 2015.

Mohammed, G. H., Colombo, R., Middleton, E. M., Rascher, U., van der Tol, C., Nedbal, L., Goulan, Y., Perez-Priego, O., Damm, A., Meroni, M. and Joiner, J.: Remote sensing of solar-induced chlorophyll fluorescence (SIF) in vegetation: 50 years of progress, Remote Sensing of Environment, 231, 111177, https://doi.org/10.1016/j.rse.2019.04.03, 2019.

Monteith, J. L.: Solar Radiation and Productivity in Tropical Ecosystems, J. Appl. Ecol., 9, 747–766, https://doi.org/10.2307/2401901, 1972.

Norton, A. J., Rayner, P. J., Koffi, E. N., and Scholze, M.: Assimilating solar-induced chlorophyll fluorescence into the terrestrial biosphere model BETHY-SCOPE v1. 0: model description and information content, Geoscientific Model Development, 11(4), 1517–1536, 2018.

Norton, A. J., Rayner, P. J., Koffi, E. N., Scholze, M., Silver, J. D., and Wan, Y.-P.: Estimating global gross primary productivity using chlorophyll fluorescence and a data assimilation system with the BETHY-SCOPE model, Biogeosciences, 16(15), 3069-3093, 2019.

Porcar-Castell, A.: A high-resolution portrait of the annual dynamics of photochemical and non-photochemical quenching in needles of Pinus sylvestris, Physiologia Plantarum, 143(2), 139–153, https://doi.org/10.1111/j.1399-3054.2011.01488.x, 2011.

Qiu, B., Chen, J. M., Ju, W., Zhang, Q., and Zhang, Y.: Simulating emission and scattering of solar-induced chlorophyll fluorescence at far-red band in global vegetation with different canopy structures, Remote Sensing of Environment, 111373, 2019.

Raczka, B., Duarte, H. F., Koven, C. D., Ricciuto, D., Thornton, P. E., Lin, J. C., & Bowling, D. R.: An observational constraint on stomatal function in forests: evaluating coupled carbon and water vapor exchange with carbon isotopes in the Community Land Model (CLM4. 5), Biogeosciences, *13*(18), 5183-5204, 2016.

Raczka, B., Porcar-Castell, A., Magney, T., Lee, J. E., Köhler, P., Frankenberg, C., Grossman, K., Logan, B.A., Stutz, J., Blanken, P. D., Burns, S. P., Duarte, H., Yang, X., Lin, J. C., and Bowling, D. R.: Sustained nonphotochemical quenching shapes the seasonal pattern of solar-induced fluorescence at a high-elevation evergreen forest, Journal of Geophysical Research: Biogeosciences, 124, 2005–2020, https://doi.org/10.1029/2018JG004883, 2019.

Rayner, P. J., Scholze, M., Knorr, W., Kaminski, T., Giering, R., and Widmann, H.: Two decades of terrestrial carbon fluxes from a carbon cycle data assimilation system (CCDAS), Global Biogeochemical Cycles, 19(2), 2005.

Schreiber, U., Schliwa, U., and Bilger, W.: Continuous recording of photochemical and non-photochemical chlorophyll fluorescence quenching with a new type of modulation fluorometer, Photosynthesis Research, 10, 51–62, 1986.

Sellers, P. J., Randall, D. A., Collatz, G. J., Berry, J. A., Field, C. B., Dazlich, D. A., Zhang, C., Collelo, G. D., and Bounoua, L.: A revised land surface parameterization (SiB2) for atmospheric GCMs. Part I: Model formulation, Journal of Climate, 9(4), 676–70, 1996.

Shan, N., Ju, W., Migliavacca, M., Martini, D., Guanter, L., Chen, J., Goulas, Y., Zhang, Y.: Modeling canopy conductance and transpiration from solar-induced chlorophyll fluorescence. Agricultural and Forest Meteorology, 268, 189–201, 2019.

Svishnikov, D., Ensminger, I., Ivanov, A. G., Campbell, D., Lloyd, J., Funk, C., Huner, N. P. A., Oquist, G.: Excitation energy partitioning and quenching during cold acclimation in Scots pine. Tree Physiology, 26(3), 325-336, 2006.

Van Der Tol, C., Berry, J. A., Campbell, P. K. E., and Rascher, U.: Models of fluorescence and photosynthesis for interpreting measurements of solar-induced chlorophyll fluorescence, Journal of Geophysical Research: Biogeosciences, 119(12), 2312–2327. https://doi.org/10.1002/2014JG002713, 2014.

Wohlfahrt, G., Gerdel, K., Migliavacca, M., Rotenberg, E., Tatarinov, F., Müller, J., Hammerle, A., Julitta, T., Spielmann, F.M., Yakir, D.: Sun-induced fluorescence and gross primary productivity during a heat wave. Sci. Rep., 8, 1–9, 2018.

Yang, P., and van der Tol, C.: Linking canopy scattering of far-red sun-induced chlorophyll fluorescence with reflectance, Remote Sensing of Environment, 209(May), 456–467. https://doi.org/10.1016/j.rse.2018.02.029, 2018.

Yin, X., and Struik, P. C.: C3 and C4 photosynthesis models: an overview from the perspective of crop modelling, NJAS-Wageningen Journal of Life Sciences, 57(1), 27-38, 2009.

Zhang, Y., Guanter, L., Berry, J. A., van der Tol, C., Yang, X., Tang, J., and Zhang, F.: Model-based analysis of the relationship between sun-induced chlorophyll fluorescence and gross primary production for remote sensing applications, Remote Sensing of Environment, 187, 145–155, 2016.

Zhang, Q., Zhang, X., Li, Z., Wu, Y., and Zhang, Y: Comparison of Bi-Hemispherical and Hemispherical-Conical Configurations for In Situ Measurements of Solar-Induced Chlorophyll Fluorescence, Remote Sensing, 11, 2642, 2019.

Figures

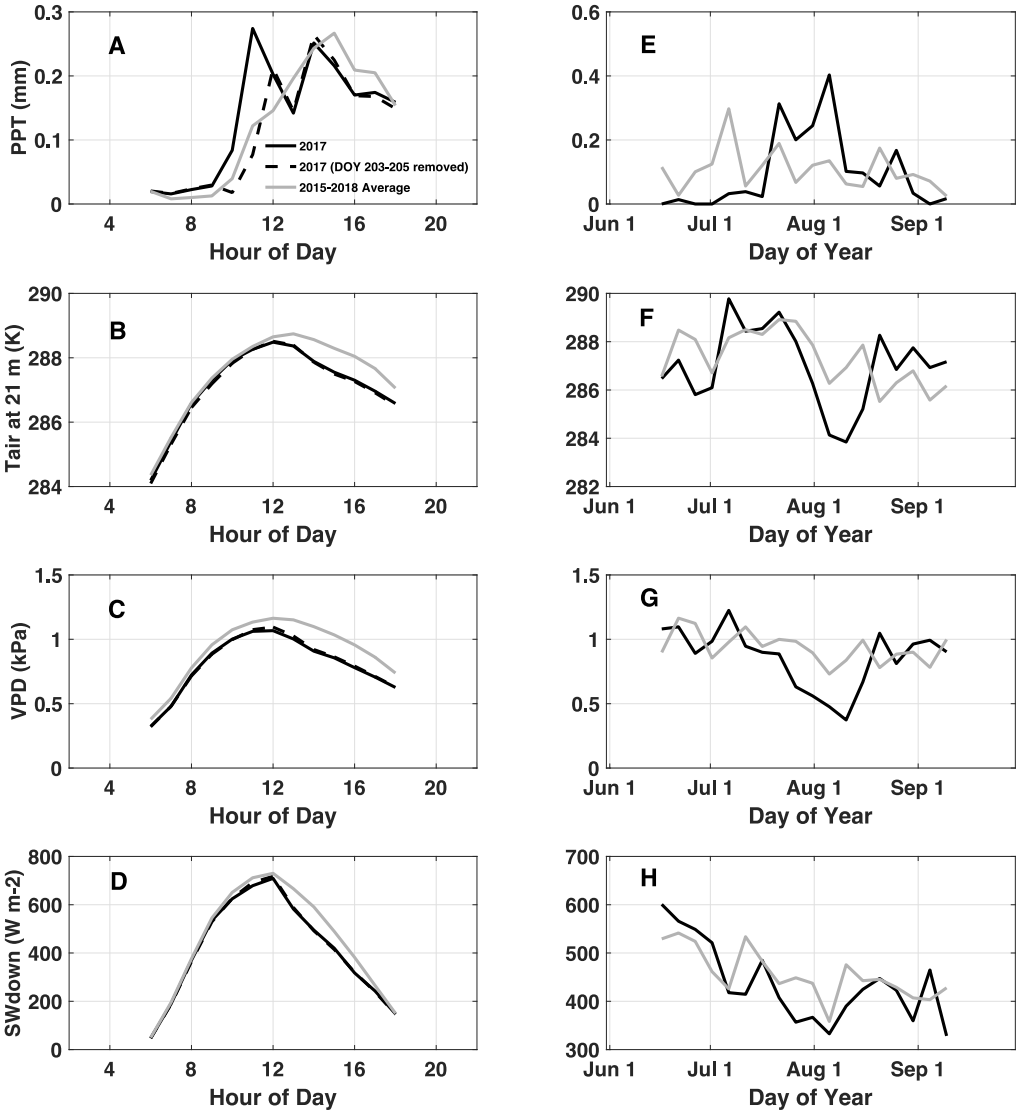

Figure 1. Observed diurnal (A-D) and synoptic (E-H) precipitation (PPT), air temperature at 21 m (Tair), vapor pressure deficit (VPD), and downwelling shortwave (SWdown). Diurnal cycles are averaged over July-August, 2017. Synoptic cycles are plotted as 5-day averages from June 15 – Sep 15. Data from 2017 is shown in black and climatology (2015-2018) in grey. Typically, peak rainfall occurs in the afternoon at this site (A). A substantial rain event which occurred from DOY 203-205 is removed from the 2017 average to show the impact on diurnal variability and to demonstrate the dominance of the afternoon monsoon upon diurnal precipitation in summer.

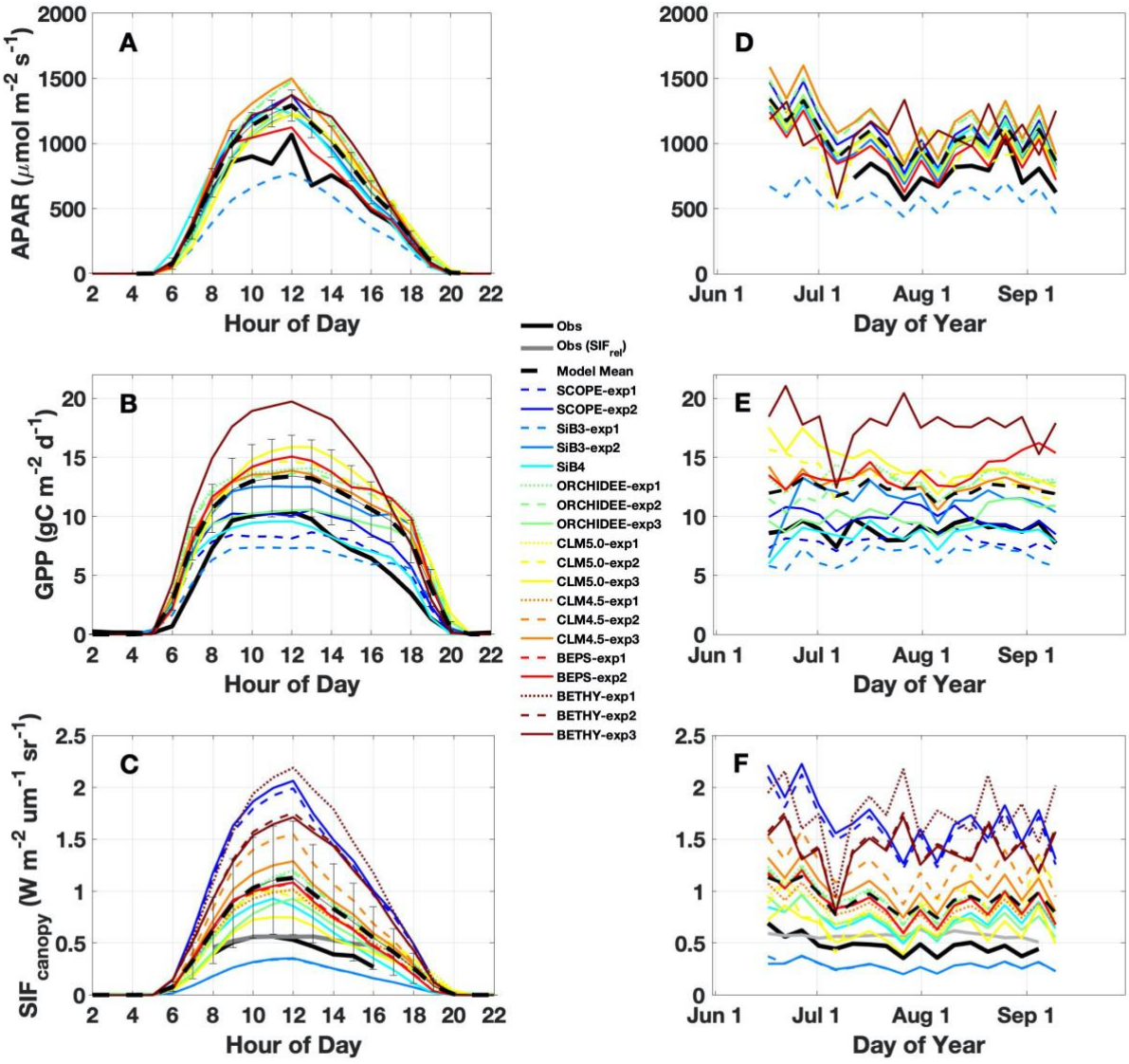

Figure 2. Observed and simulated diurnal and synoptic cycles of APAR, GPP and SIF. Diurnal cycles (A-C) are averaged over July-August, 2017. Synoptic cycles (D-F) are plotted as 5-day averages from June 15 – Sep 15. Observations are shown in black, with relative SIF (SIF_{canopy} / far red reflected radiance) included in (C, F) in grey. The across model average (dashed black) represents the average of "best-case" model scenarios (solid lines; SCOPE-exp2, SiB3-exp2, SiB4, ORCHIDEE-exp3, CLM5.0-exp3, CLM4.5-exp3, BEPS-exp2, BETHY-exp3) with uncertainty bars indicating the across model 1 sigma uncertainty.

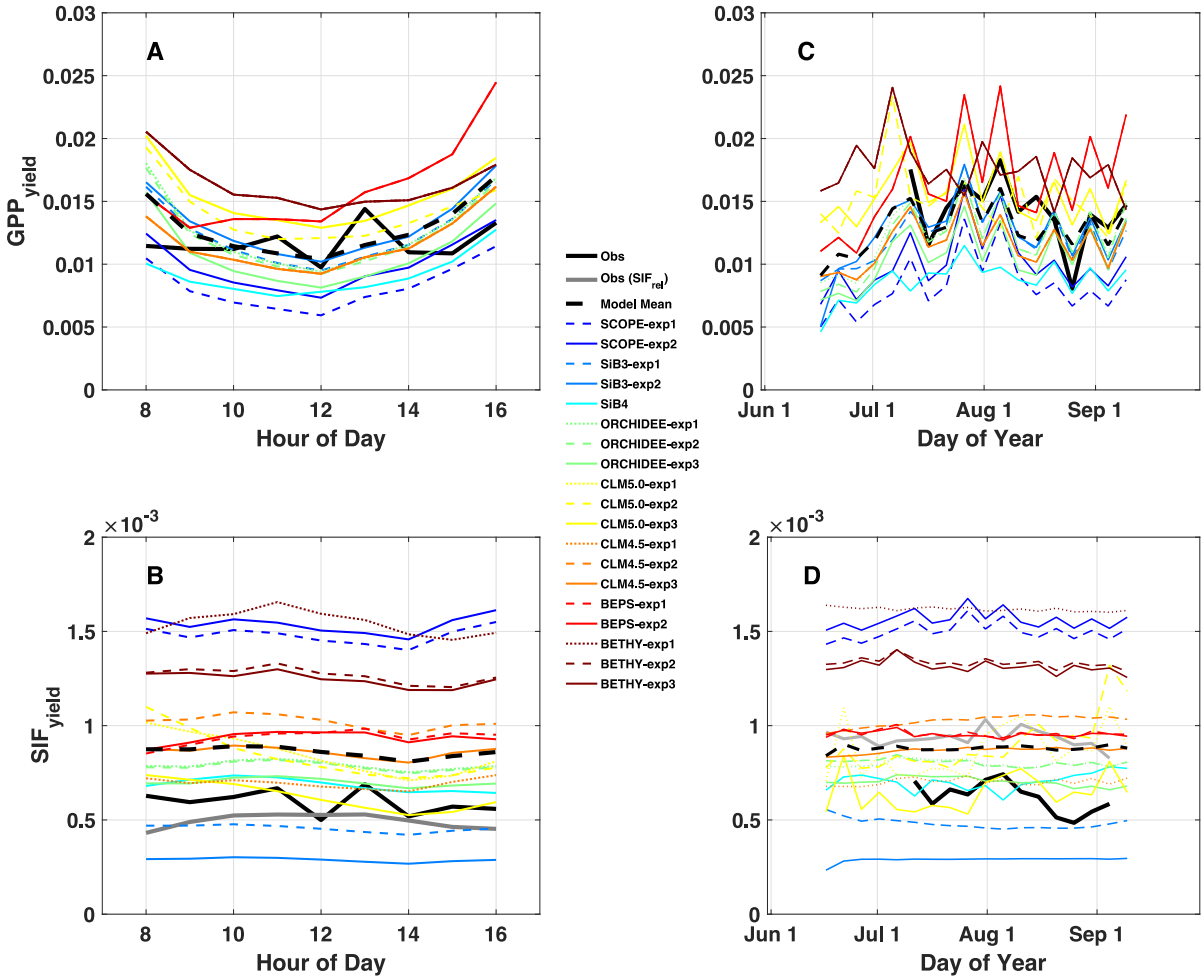

Figure 3. Same as Figure 2 except for SIF_{yield} and GPP_{yield}. Here, SIF_{yield} = SIF_{canopy} / APAR, and GPP_{yield} = GPP / APAR. As with Figure 2, the left column shows the mean diurnal cycle, and the right column shows a time series of 5-day averages.

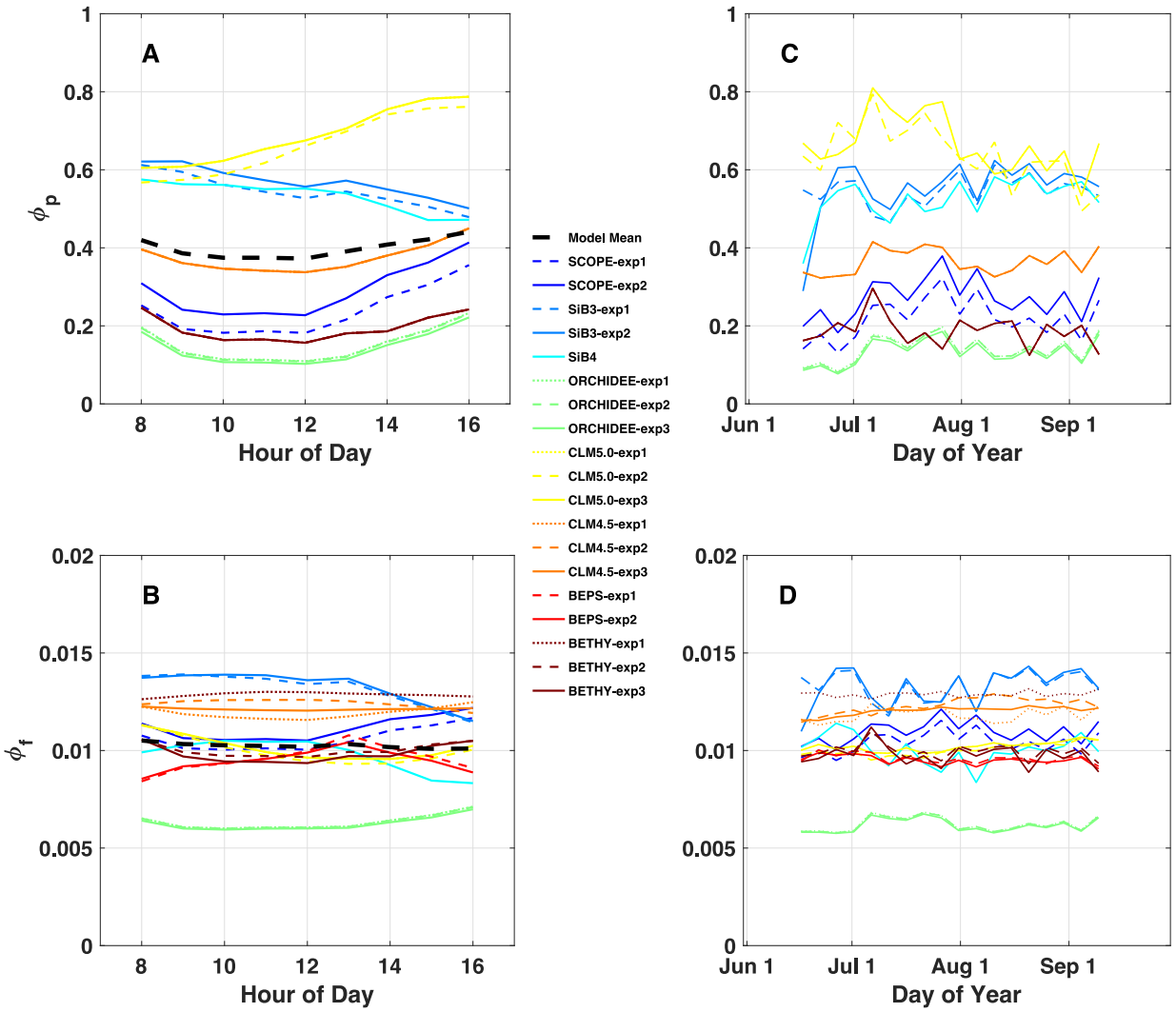

1167

1168 **Figure 4**. Same as Figure 2, except for quantum yield of fluorescence (ϕ_F) and photochemistry

1169 (ϕ_P).

1170

1171

1172

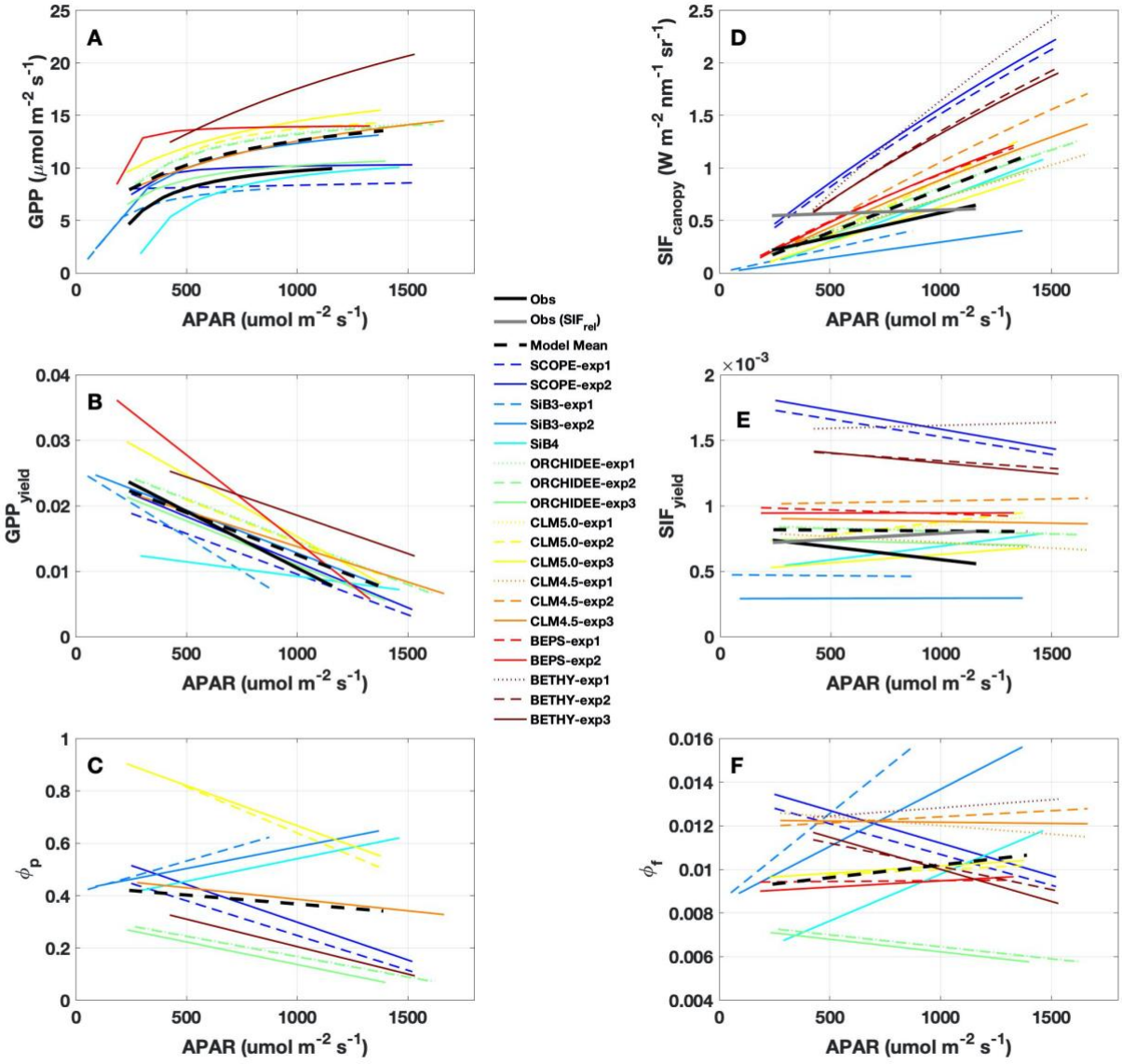

Figure 5. Observed and predicted change in GPP, SIF, and yields with APAR. Regression lines are shown for (A) GPP, (B) GPP_{yield}, (C) photochemical quantum yield (ϕ_p), (D) SIF_{canopy}, (E) SIF_{yield}, (F) fluorescence quantum yield (ϕ_f), as a function of APAR, using daily mean (8 am – 4 pm local) values over the period July-August 2017. Observations are shown in solid black, individual models and experiments in color, the across model average in dashed black. Relative SIF is shown in grey in (D) and (E).

Tables

Model (citation)	Model Experiments	Stomatal Conductance	Canopy Type / Radiation	Stress	Vcmax	LAI	k_N	Leaf-to-Canopy Scaling	Parameter Optimization
SCOPE v1.73 (van der Tol, 2014)	SCOPE-exp1	Ball-Berry-Woodrow	Multi-layer Sunlit/Shaded = Yes Fpar/APAR = semi-analytical canopy radiative model (based on SAIL)	Ta stress	Prescribed (30)	Prescribed (4.0 m^2 m^{-2})	Adapted to drought stressed Mediterranean species including high temperature correction (Tol et al., 2014; Flexas et al., 2002)	60 layer 1D radiative transfer	Hand-tuned to NR1 (Raczka et al., 2016)
	SCOPE-exp2				Seasonally calibrated to NR1				
BETHY (Norton et al., 2019)	BETHY-exp1	Ball-Berry-Woodrow	Same as SCOPE	Ta stress	Prior is a function of Ta	Prescribed (4.0 m^2 m^{-2})	Adapted to unstressed cotton species (Tol et al., 2014)	SCOPE radiative transfer. f(Ta, APAR, structure, leaf composition) via dependence of photosynthetic rate on ϕ_f	Default
	BETHY-exp2						Adapted to drought stressed Mediterranean species including high temperature correction (Tol et al., 2014; Flexas et al., 2002)		
	BETHY-exp3						Adapted to drought stressed Mediterranean species (Flexas et al., 2002)		
ORCHIDEE (Bacour et al., 2019)	ORCHIDEE-exp1	Yin-Struik	Big Leaf Sunlit/Shaded = No APAR = Beer-Lambert law depending on LAI and extinction factor = 0.5	Ta stress	f (leaf age, CO_2, Ta, water stress)	Prognostic	Adapted to needleleaf species (Porcar-Castell et al., 2011) and unstressed Mediterranean species (Flexas, 2002), with added dependence on PAR, temperature, and ϕ_P	Parametric representation of SCOPE (v1.61) to emulate radiative transfer within canopy for PSI/II.	Default
	ORCHIDEE-exp2			Ta and water stress (Yin and Struik, 2009)					Default
	ORCHIDEE-exp3			Same as exp 1					Global ENF PFT optimized against OCO-2
BEPS (Qiu et al., 2019)	BEPS-exp1	Leuning	Two Leaf Sunlit/Shaded = Yes Fpar = semi-analytical canopy radiative transfer	Soil water stress factor (ratio of measured soil available water to maximum plant available water)	Prescribed	Prescribed (4.0 m^2 m^{-2})	Adapted to water stressed Mediterranean species (Galmes et al., 2007)	Parametric representation of radiative transfer physics to account for canopy scattering effects	Default
	BEPS-exp2						Adapted to drought stressed Mediterranean species including high temperature correction (Tol et al., 2014; Flexas et al., 2002)		
CLM4.5 (Raczka et al., 2019)	CLM4.5-exp1	Ball-Berry-Woodrow	Two Big Leaf Sunlit/Shaded = Yes	Ta(Vcmax); soil moisture stress uses Btran parameterization (function of column rooting profile and soil water potential)	Prescribed (calibrated against observed GPP at NR1)	Prescribed (4.0 m^2 m^{-2})	Adapted to water stressed Mediterranean species (Galmes et al., 2007)	κ_{740} = f(Vcmax, SZA), calibrated to offline SCOPE runs using prescribed canopy characteristics at NR1	Hand-tuned to NR1 (Raczka et al., 2016)
	CLM4.5-exp2						Adapted to needleleaf species (Porcar-Castell et al., 2011); Accounts for sustained NPQ (k_S) separately from reversible NPQ (k_R). k_S is calibrated to NR1 Tair. k_R is fixed in time		
	CLM4.5-exp3						same as Exp 2, but k_R is seasonal		
CLM5.0 (unpublished)	CLM5.0-exp1	Medlyn	Two Big Leaf Sunlit/Shaded = Yes	Plant hydraulic water stress (Sperry and Love, 2015; Lawrence et al., 2019) accounting for water demand and supply	f (soil moisture, nitrogen), calibrated to NR1	Prescribed (4.0 m^2 m^{-2})	Adapted to water stressed Mediterranean species (Galmes et al., 2007)	κ_{740} = f(Vcmax), calibrated to offline SCOPE runs from Lee et al. (2015)	Default
	CLM5.0-exp2							κ_{740} = f(Vcmax, SZA), calibrated to offline SCOPE runs w/ prescribed canopy characteristics at NR1	
	CLM5.0-exp3							Escape ratio (f_{esc}), derived from NIRv and fPAR (Zeng et al., 2019)	
SiB3 (Baker et al., 2003, 2008) SIB4 (Haynes et al., 2019a,b)	SiB3-exp1	Ball-Berry-Woodrow	Big Leaf Sunlit/Shaded = No	Downregulation by VPD, Ta, and soil moisture	f (soil moisture)	Prescribed (MODIS)	Adapted to drought stressed species (Tol et al., 2014)	κ_{740} = f(Vcmax), calibrated to offline SCOPE runs from Lee et al. (2015)	Default
	SiB3-exp2					Prescribed (4.0 m^2 m^{-2})			
	SiB4					Prognostic			

Table 1. Summary of TBM-SIF models and within model experiments illustrating model components that may have led to differences in modeled SIF., These include a representation of stomatal-conductance (column 3), canopy absorption of incoming radiation (column 4), limiting factors for photosynthesis (Stress, V_{cmax}, LAI; columns 5-7) and SIF (k_N; column 8), leaf-to-canopy scaling of SIF (column 9), and parameter optimization (column 10). The underlined model experiment was used for model intercomparison .